Trabajo Fin de Máster
Máster Universitario en Ingeniería Industrial

Analysis of an Electrical Energy Storage System Based on Flow Batteries

Autor: Elisa Hidalgo Moreda

Tutor: José Alfredo Iranzo Paricio

Dpto. Ingeniería Energética
Escuela Técnica Superior de Ingeniería
Universidad de Sevilla

Sevilla, 2023

Trabajo Fin de Máster
Máster Universitario en Ingeniería Industrial

Analysis of an Electrical Energy Storage System Based on Flow Batteries

Autor:
Elisa Hidalgo Moreda

Tutor:
José Alfredo Iranzo Paricio
Profesor Ayudante Doctor

Dpto. Ingeniería Energética
Escuela Técnica Superior de Ingeniería
Universidad de Sevilla

Sevilla, 2023

Trabajo Fin de Máster: Analysis of an Electrical Energy Storage System Based on Flow Batteries

Autor: Elisa Hidalgo Moreda
Tutor: José Alfredo Iranzo Paricio

El tribunal nombrado para juzgar el trabajo arriba indicado, compuesto por los siguientes profesores:

Presidente:

Vocal/es:

Secretario:

acuerdan otorgarle la calificación de:

El Secretario del Tribunal

Fecha:

Acknowledgements

I pay tribute to my family and friends for the massive motivation and patience that have infinitely helped me stay focused. Special thanks to my tutor for the ongoing support as well as the invaluable amount of trust placed in me. It is only thanks to these people I have managed to accomplish this research project and the many years of intensive work ethic behind it. However, I would also like to express gratitude for the lessons learnt through this project, which I hope to never forget in the future. I have learnt to grasp opportunities behind visible difficulties. I genuinely hope to extend this mindset to other areas in my personal and professional life ahead.

Elisa Hidalgo Moreda
Sevilla, 2023

Resumen

En el contexto de una transición del modelo eléctrico y energético, este proyecto pretende explorar en detalle una tecnología prometedora: las Baterías de Flujo Redox desde múltiples puntos de vista. En primer lugar se presenta una introducción sobre el interés de estos sistemas: por qué los científicos buscan nuevos sistemas de baterías y qué pueden aportar las RFB en particular al escenario actual.

Una vez expuesto esto, se examina el principio de funcionamiento y los componentes de las baterías de flujo redox. Comprender en profundidad cómo funciona el sistema permitirá llevar a cabo una investigación aún más amplia sobre el estado del arte de las baterías de flujo redox.

Así, en la sección Líneas de investigación y retos se exponen las diferentes líneas de investigación, los retos encontrados y, en consecuencia, la forma en que se lideran futuras investigaciones.

Por último, se realiza un estudio de viabilidad económica para evaluar la viabilidad potencial de este tipo de baterías en el mercado. Este estudio se basa en un sistema ya instalado en Japón, cuya estabilidad a largo plazo ha sido demostrada. Adicionalmente, se evalúa la viabilidad de dicho sistema hipotéticamente conectado a la red eléctrica española mediante un análisis de costes jerárquico e incremental, que tiene en cuenta múltiples factores.

Finalmente, este trabajo concluye que existe una amplia variedad de áreas de investigación aún abiertas y que se requiere más investigación para encontrar la combinación ideal de los diferentes elementos en una RFB (electrolitos, electrodos, membranas, etc.) que logren demostrar estabilidad a largo plazo así como una eficiencia alta. Por el momento, la inclusión de las baterías de flujo redox en España no parece viable en términos económicos, debido a las limitaciones de la red y a los elevados costes de inversión inicial para producir todo el sistema.

Abstract

In the context of an electrical and energy model transition, this project aims to explore in detail a promising technology: Redox Flow Batteries from multiple points of view. In the first place, an introduction regarding why these systems are interesting is presented: why scientists seek new battery systems and what RFBs in particular can add to the current scenario.

That being exposed, the working principle and components of Redox Flow Batteries is examined. Deeply understanding how the system works will allow for an even more extensive research to be carried out, regarding the State of Art of these systems.

In this way, the Research Lines and Challenges section puts forward what different research lines have been tackled, the challenges encountered, and as a result, the way in which further investigations have been led.

Lastly, an economic feasibility study is conducted to assess the potential viability of this type of battery in the market. This study is based on a system already installed in Japan, whose long-term stability has been proven. Additionally, the feasibility of such system hypothetically connected to the Spanish electrical network is assessed through a hierarchical and incremental cost analysis, that takes into account multiple factors.

This work finally concludes there is a wide variety of investigation areas still open and further research is required in order to find the ideal combination of the different elements in a RFB (electrolytes, electrodes, membranes, etc.) that proves to show long-term stability as well as efficiency. As of now, including redox flow batteries in Spain seems not to be feasible in economic terms, due to the limitations in the network and the high initial investment costs to produce the entire system.

Contents

1 Introduction

This chapter tackles why research focus has been driven towards Redox Flow Batteries. In order words, it highlights the main reasons as to why researchers find interest in this type of technology. In the same way the pursued applications for this type of system are briefly commented.

1.1 Interest

Energy is the raw material that sustains human life and contributes to the development of industrialization and lifestyle. As digitalization takes over along with technological development and electrification, more energy consumption is being registered. The trend, as shown in Figure 1.1 could even be described as exponentially increasing.

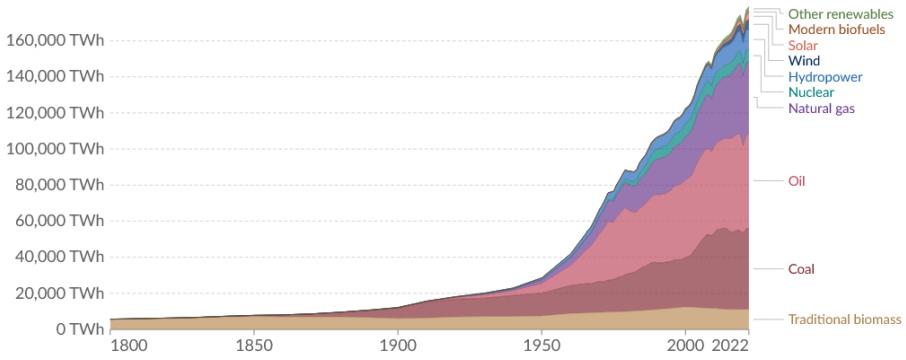

Figure 1.1 Global primary energy consumption by source [51].

This Figure puts forward how oil and coal are the sources most primary energy consumption reports to. The nineteenth century increase in energy consumption is pretty much negligible, when compared to the increase incurred through the twentieth century. In fact in less than a hundred years (from 1950 to 2022) energy consumption has increased by more than a factor of four.

The reality is that as can be seen in Figure 1.1, this rise in demand has been palliated through the exploitation of fossil fuel energy sources (e.g. coil and oil). This poses foreseen obstacles, which are exposed hereinafter [52].

In the first place, fossil fuel prices are sharply rising due to the scarcity of this source and the associated complication of extracting energy out of them.

Additionally, fossil fuels strongly contribute to contamination and climate change, due to the greenhouse gases emission produced when burning them in order to get energy from them.

This, followed by the growing demand of energy pointed out before, makes scientists seek for alternative energy sources. Specifically, renewable energies as they have the potential of being natural energy sources able to produce energy indefinitely. Renewable energy sources have almost no negative impact on the environment, they are "clean energy". Nonetheless, they behave in a very random and unpredictable way. For instance, wind energy depends on the speed of wind as much as photovoltaic sources rely on solar radiation to generate usable energy. This is where it becomes vital to use systems that are able to store energy, like batteries, thereby increasing economic feasibility of energy production through renewable sources. This is a promising scheme capable of balancing energy offer and demand.

There are multiple renewable energy sources that can later be stored through battery systems, such as but not limited to [52]:

- Solar energy
- Wind energy
- Hydraulic energy
- Seawater energy
- Geothermic energy
- Energy from biomass and waste

Since renewable energy sources are not the study matter of this project, no further emphasis will be made on them. It is also important to note that as much as there are multiple energy sources, there are also a vast variety of ways to store energy like capacitors, compressed air or fuel cells.

Again multiple batteries co-exist in the electrochemical storing market, such as lead-acid or lithium-ion. However, what differentiates redox flow batteries from other battery types is:

- Their ability to physically increase/decrease power and capacity in an independent manner
- Low self-discharge level
- Promisingly low degradation level due to the chemical principles they obey

Still a lot of research has to be carried out on this battery system type for it to be feasible and useful in its required applications, as will be presented in this work. However, they are a valid candidate to aid decarbonization of the electric sector [52].

1.2 Possible applications

RFBs are low density battery systems, so they have not been considered for mobile systems but rather stationary ones. However, their ability to have energy and power uncoupled is seemingly interesting. Some of the possible applications of conventional batteries likewise apply to RFBs. For instance:

- **Load leveling.** They store energy in periods of excess and consume it in periods when the price of energy is higher. As a result, making the cost of energy more economical.
- **Smoothing and power regulation.** VRFBs are used to smooth the power peaks that occur due to high energy consumption.

- **Uninterruptible voltage generators.** Due to their short response time and long discharge cycles, these batteries come on line when there is a failure in the generation systems, thus avoiding serious failures in the electrical grid and the cost that this would entail.
- **Combination with renewable energies**. The large number of useful life cycles of VRFBs, up to 20 years in some cases, makes them ideal to compensate for the intermittency and poor stability of clean energies.

Already by 2010, Skyllas et. al accounted for multiple live applications of redox flow batteries. [58] Some of them are summarized in Table 1.1.

Table 1.1 Example applications of existing RFB systems.

Power (kW)	Capacity (kWh)	Country	Year	Application
200	800	Japan	1996	Load-levelling
200	1600	Japan	2000	Peak-shaving
250	500	South Africa	2001	UPS back-up power
4000	6000	Japan	2005	Wind energy storage and wind power stabilization

Next chapter will dive into the working principle of Redox Flow Batteries. This settles the basis to then understand most common research and development challenges encountered through the literature.

2 Working principle of Redox Flow Batteries

The research topic of redox flow batteries has been a fairly inviting one over the years. As previously alleged, they hold great promise for addressing the challenges posed by the transition to a renewable energy future along with other battery energy storage systems. This last statement raises the question of what exactly has the potential to put RFBs at an advantage when compared to other battery types. Although finding a concrete answer to this enquiry is complex, it is possible to draw a set of conclusions by merely examining this batteries' working principle.

As suggested by their name, RFBs work thanks to the occurring redox chemical reactions in them. To begin with, their working principle will be outlined with the help of Figure 2.1.

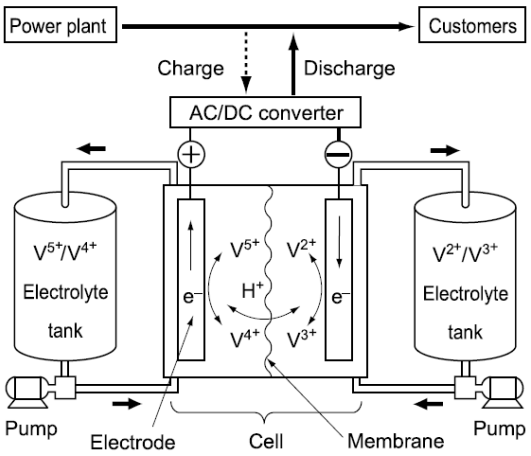

Figure 2.1 Working principle of RFBs [67].

While the scheme presented in Figure 2.1 shows an all-vanadium system, the parts or components are equivalent regardless of the compounds taking part in the reactions. As seen in this diagram, the key components that must be present are:

- **Positive electrolyte** (generally also known as catholyte)
- **Negative electrolyte** (generally also known as anolyte)
- Two **tanks** to store both electrolytes
- Two **pumps** integrated in a flow control system

- **Membrane**
- Two **electrodes**

From Figure 2.1, it can be depicted that the electrolytes are pumped through a battery cell where power can be put into or taken out of the fluids by changing their oxidation states. Since charging and discharging occurs in the stacks, the latter are directly related to the quantity of power that the system is able to supply.

This point can be emphasized by affirming that the design is modular [35]:

- If more energy is required to be stored in the system, the size of the tanks can be increased,
- whereas if there is a higher requirement of power, more stacks can be added

Figure 2.2 below shows a visual representation of a cell stack. As it can be seen, cells are stacked in both serial and parallel connections. Piling them up in series increases the voltage, while piling them up in parallel allows the obtention of a greater current.

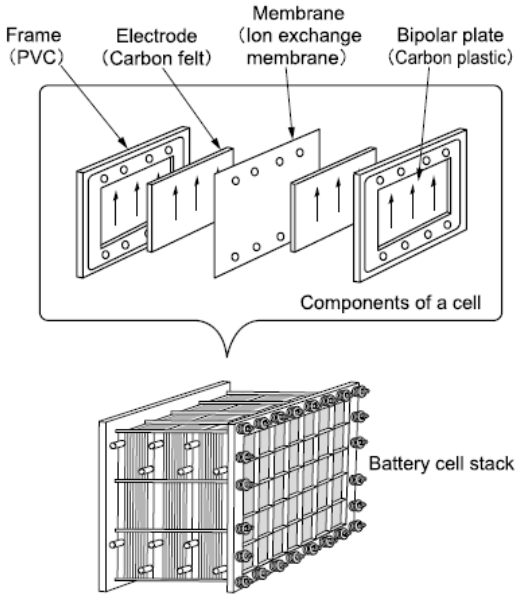

Figure 2.2 Construction of a cell stack [67].

To understand this architecture in detail, this chapter will be broken down into two main sections. Section 2.2 will explore how and where redox reactions occur inside the cell allowing its operation. On the other hand, Section 2.1 will focus on thoroughly analysing the rest of the system.

2.1 Main components

Redox flow batteries consist of several essential components that work together to store and release energy. These components include:

2.1.1 Electrolyte tanks

Redox flow batteries use two separate tanks to store the two different electrolytes: anolyte and catholyte. Their design must be done in order to contain and store the electrolyte content safely. As explained below the design of a Redox Flow Battery is modular:

- Energy is directly related to the size of the tanks

- Power can be increased by considering a higher number of stacks

The reason why energy is said to be related to the size of the tanks is because having more voluminous tanks allows for more electrolyte to be stored. The active species here are the electrolytes. Thus the capacity of the battery turns out to be directly proportional to the amount of active species that are accessible to take place in the occurring electrochemical reactions.

This statement is inherently materialized through real applications. Figure 2.3 shows a 60kWh Redox Flow Battery System (tanks being by the side of the system). The purpose of such all-vanadium battery is to integrate it with rooftop photovoltaic panels (PV). [7] On the other hand Figure 2.4 puts forward one of the Redox Flow Battery systems with highest battery capacity worldwide. This iron-chromium RFB was developed by Enervault and is even connected to the grid in such a way that it's able to inject energy back to it during times of high demand.

Figure 2.3 60 kWh- equivalent tanks [7].

Figure 2.4 1 MWh- equivalent tanks [48].

Regarding materials, not every single one is valid to build electrolyte tanks. In fact, the material used for the electrolyte tanks depends on multiple factors such as but not limited to chemical compatibility, cost or the ease of production.

Some common materials employed may be:

1. High-density polyethylene (HDPE)
2. Polypropylene (PP)- *poly tanks*
3. Glass-reinforced plastic (GRP)- *fiberglass tanks*
4. Stainless steel

For example, Figure 2.12 implicitly informs that sulphuric acid is stored in the tanks in this all-vanadium system equations. Henceforth, the tank must be made of corrosion-resistance materials. Otherwise the security, longevity or stability of the tank may be compromised. [15] [1]

If the commonly known Polypropylene and glass-reinforced plastic tanks were to be compared, it is notable that:

- GRP tanks are handmade. As a consequence it is subjected to human error in the course of its production. On the other hand, PP tanks' manufacturing process is automated.
- GRP are costly to make, polyethylene/polypropylene tanks are less expensive
- Due to the corrosion resistance of poly storage tanks, maintenance is less burdensome

In the light of such facts, the market trends are directed towards considering poly tanks as opposed to fiberglass ones.

2.1.2 Electrodes

Likewise electrolytes, electrodes of Redox Flow Batteries can be of two types: positive electrode or negative electrode. The positive one (cathode) is liable for the oxidation reaction, while the negative electrode (anode) facilitates the reduction reaction. Note that the type of reaction (oxidation or reduction) is being denoted taking into account the battery being discharged. Refer to Figure 2.9 and Equations 2.1 and 2.2.

Regarding sizes, we may encounter that the size of one side of an electrode vary in the order of the tens *cm*. That is to say that the surface area of the electrodes (magnitude of interest as it will be drawn later on through this Section) will be in the order of the hundreds or thousands cm^2. This will depend on the casuistry and application. Thielke carried out experiments with $125cm^2$ surface area electrodes [64], while the IMDEA Energy Institute research group has worked with electrodes as big as $1800cm^2$ each. [18]

Anyhow, the distinction of the electrode being "positive" or "negative" only has to do with them being in direct contact with the catholyte or anolyte respectively. In reality, both anode and cathode are generally made from the same materials. This presents multiple advantages such as cost reduction or simplification of the manufacturing process. There can still be exceptions, where the anode and cathode are made of different materials so as to optimize concrete performance characteristics. Some of the most common materials for electrodes can, for instance, be:

- Graphite
- Carbon felt
- Conductive ceramics
- Mixed- metal oxides

As it can be depicted from the previous list of examples, the electrodes must be highly conductive materials as it is through them that the electrons will flow in order to charge and discharge the battery. Likewise the higher the surface area of the electrodes, the more enhanced the electrochemical reaction as they provide "the reaction sites" [10]. They accommodate more active material improving the speed of electron transfer.

An important point to emphasize is that electrodes are "inert" [10] and their main function is to be the bridge to enable electron flow. Thus the electrodes must exhibit rapid kinetics of the redox

couple reactions so that the energy efficiency and voltage of the system is optimized as much as possible. As much as the kinetics for these reactions must be fast, the kinetics of reactions that could produce hydrogen and oxygen at them must be slow, so that undesirable side reactions are inhibited.

In view of this there have been research lines focused on intrinsic and catalytic treatments for both anodes and cathodes over time.

Intrinsic treatments

Intrinsic treatments aim to improve the performance of the electrodes in the whole energy storage system.

These may include [21] among others:

1. Thermal treatment
2. Acid treatment
3. Chemical etching
4. Heteroatom doping
5. Microwave treatment

Next, this research work will delve into them.

Thermal treatment proves to be one of the most appealing methods for improving the electrodes performance, since given optimum conditions of temperature and time exposure functionalization of electrodes takes place. It results in improvement of the cell's efficiency as oxygen-based functional groups are generated (this is also related to wettability). [6] In this way, many experiments were carried out. For instance, Skyllas-Kazacos [62] tested out a thermal treatment upon graphite felt for VRFB, findinf out that its energy efficiency increased by 10% after treating it at 400 degrees Celsius for thirty hours thanks to the formation of C-O-H and C=O functional groups on its surface. This effect accelerated electron transfer, thus increasing energy efficiency. Likewise, [20] found out the optimum pre-treatment temperature for GF to be 475 degrees Celsius.

Acid treatment, on the other hand, has multiple advantages as well like good oxidation effect, simple operation and cost effectiveness. Li et Al ,Sun et Al treated carbon paper with mixed acid under the action of ultrasonic wave, and obtained a hydroxylated electrode [77]. Increasing treatment time increases the number of functional groups that enable active sites for reaction, yet the mechanical strength is worsened.Besides, excess functional oxygen group can increase resistance decreasing the conductivity of electrons at the electrodes.[77] Therefore, it becomes crucial for time of these treatments to be controlled.

Chemical etching aims to increase specific surface area in carbon-based materials. A successful technique is KOH etching, which has been used in multiple manners to form pores, increasing the number of active sites for fast electrochemical reactions. In [79] a dual-scale porous electrode was developed with different size pores, presented in Figure 2.5, all thanks to KOH activation of the fibers of carbon papers:

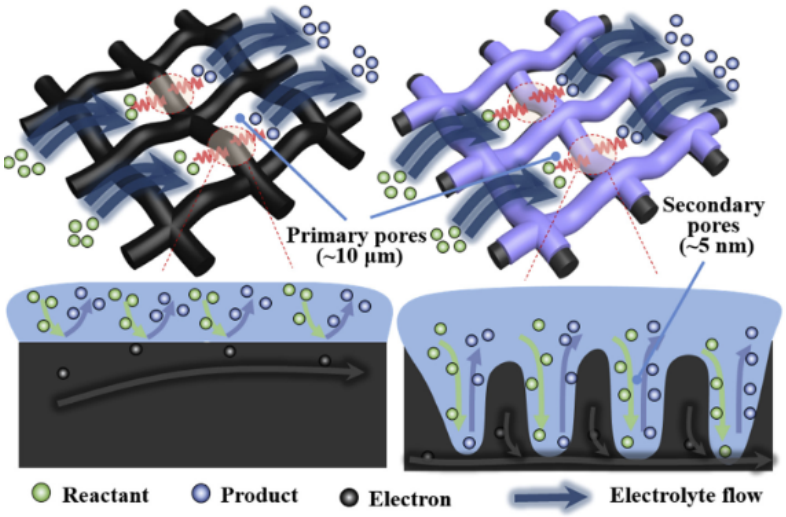

Figure 2.5 The schematic of the conventional carbon-fiber based electrode and the proposed dual-scale porous carbon electrodes [79].

Heteroatom doping involves doping organic compounds with nitrogen, phosphorous, or boron among others. Perhaps the most mature technology may be doping N into carbon-based materials. This enhances the electrodes performance in multiple ways- improving electrode activity as well as improving the reversibility of VO^{2+}/VO_2^+ on the electrode. Researchers have found that co-doping of nitrogen and oxygen futher promotes the redox reaction of vanadium ions than doping with oxygen or nitrogen atoms alone. Diverse studies have been carried out on this regard. As an illustration, Flox et al. [32] studied the optimum reaction time and temperature for the exposure of GF to NH_3/O_2 (1:1) atmosphere revealing that subjecting graphite felt to this environment at 773K and 24 hours made it obtain the highest nitrogen and oxygen content and the best catalytic activity when utilized under an all-vanadium electrolyte (VO^{2+}/VO_2^+).

Lastly, microwave treatment prompts the heating process of the electrode and it allows for a precise control on this process. This treatments acts increasing both the functional group content and the specific active surface area; these two effects combined greatly increase the energy efficiency of the RFB.

Catalytic treatments

For a comprehensive illustration of a catalytic treatment, firstly it is convenient to review the principle behind them. Refer to Figure 2.6. Skyllas-Kazacos studied the effects of adding surface oxygen functional groups on the carbon electrode surface. "Detailed X-ray photoelectron spectroscopy (XPS) analysis confirmed that improved cell performance was associated with an increase in the oxygen functional groups on the surface of the carbon electrode, especially phenolic functional groups, which provide active sites that catalyze both the anolyte and catholyte redox reactions in an all-vanadium system" [30].

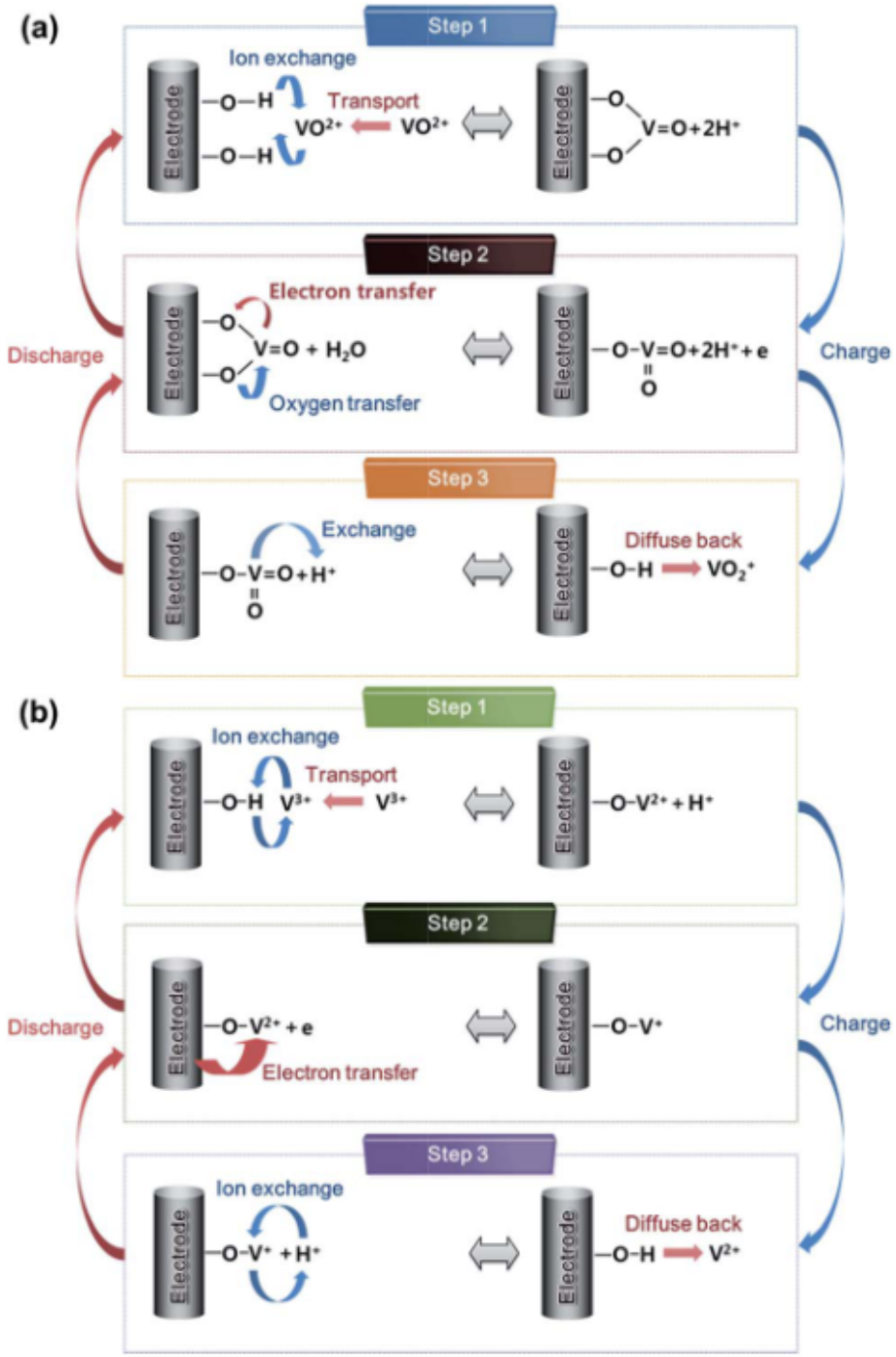

Figure 2.6 Addition of surface oxygen functional groups to electrodes [30].

Such finding induced further investigations by other researchers. Yan et al. developed a graphite/-graphite oxide composite electrode with several oxygen functional groups in it (on the basal planes and sheet edges of the GO). [33] For instance:

- Ether
- Ester
- Carbonyl

The schematic drawings of the catalytic reaction mechanisms on a graphene oxide electrode is put forward on Figure 2.7. Figure 2.7 a) illustrates the redox reaction occurring at the surface of the anode, whereas Figure 2.7 b) represents the one taking place at the cathode's surface.

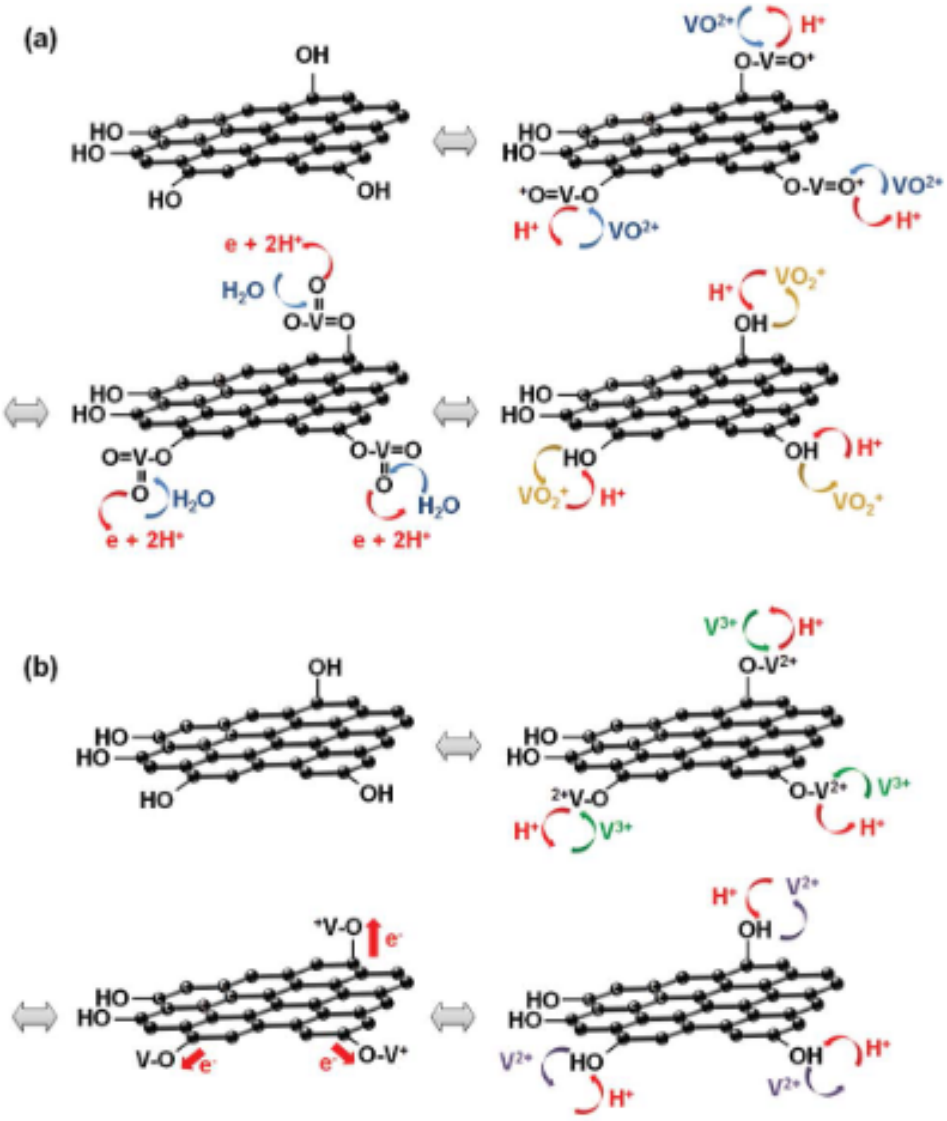

Figure 2.7 Example of enhanced mechanism due to catalytic treatment [30].

Some authors may consider adding oxygen functional groups to electrodes an intrinsic treatment called *electrochemical treatment* [21] or similar. However, for the purpose of this thesis, it will be referred to as a catalytic treatment since it speeds up the reaction rate by altering the electrode chemical structure. Other catalysts that may be introduced similarly include [21]:

- Metal
- Metal compounds
- Carbon- based materials
- Other catalysts such as C_3N_4 or B_4C

2.1.3 Ion-selective membrane

An ion-selective membrane holds its place between the positive and negative electrodes in a Redox flow battery. This membrane allows for electrons to flow through it while preventing the mixing of the two electrolytes (anolyte and catholyte).

The ion-selective membrane plays a crucial role in maintaining charge separation and preventing cross-contamination of the electrolytes.

Below, Figure 3.1 presents a classification of the different membrane types. IEMs are the most extensively used ones, especially anion-exchange membranes.

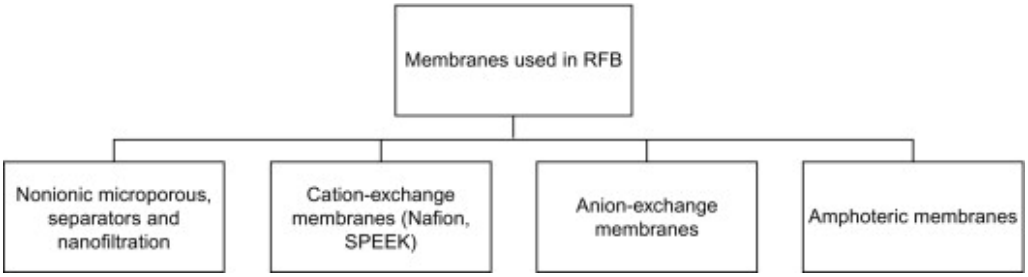

Figure 2.8 Membrane classification [34].

2.1.4 Pumping system

Another necessary device in a redox flow battery solution is a pumping system. Without it, it would not be possible to circulate the electrolytes between the tanks and the electrodes. The pumps ensure a continuous and regulated flow of electrolytes through the respective half-cells during the charging and discharging processes. The pumping system, accompanied by an efficient control system, maintains the flow of electrolyte through the cell stacks controlling the rate of reactions. A good control algorithm exerted on them ensures efficient energy storage and release.

2.1.5 Current collectors

Current collectors are conductive materials that collect the electrical current generated during the electrochemical reactions at the electrodes. These collectors are connected to external circuits, allowing the flow of electrons between the battery and the load, enabling the utilization of stored energy.

All in all, Redox flow batteries are the combination of all the aforementioned components. It is such combination that enables the conversion of electrical energy into chemical energy (charging process) and viceversa (discharging process). The separation of the energy storage medium (electrolyte) from the energy generation components (electrodes) is a distinguishing feature of Redox flow batteries. It is this feature that endows this battery type with flexibility in terms of capacity, scalability, and cycling efficiency.

2.2 Electrochemical concept

There is a broad set of options of electrolytes researched and the most investigated ones will be tackled in future chapters of this work. However, for the purpose of simplicity, from now on and through the course of this chapter, the all-vanadium system will be considered to elaborate on the working principle of RFBs. Although the reactions differ from one system to another, the oxidation and reduction reactions that charge/discharge the battery system take place analogously across them all.

This section focuses on what is tagged as *Cell* in Figure 2.1. Figure 2.9 represents in a diagram an all-vanadium system. In it, the mechanisms of oxidation and reduction as well as electron and hydrogen cation flow are portrayed.

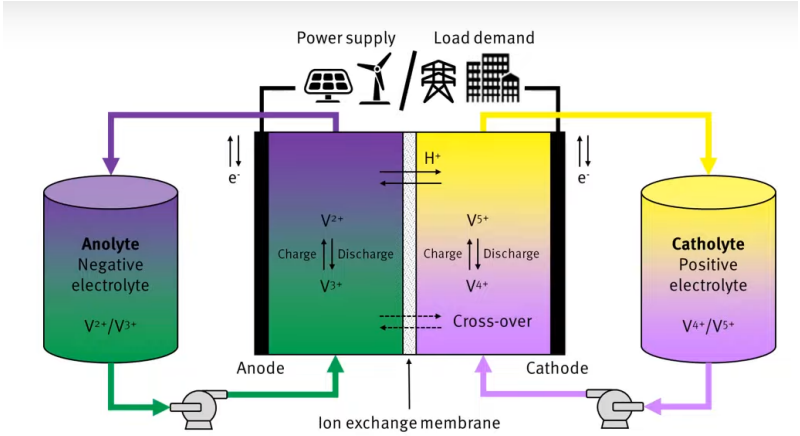

Figure 2.9 All-vanadium system [35].

If we look closely at the cross-section of an RFB cell (Figure 2.10) we can see various components:

- The electrodes can be a porous carbon electrode at both sides; often made of carbon papers or carbon felt. This allows for the electrolyte to diffuse through the cell and also provides electronic conduction pathways.
- These two porous electrodes are separated by an ion-exchange membrane which doesn't allow for electrolytes nor electrons to flow through but it does allow for charge carriers to pass. In the upcoming chapters, diverse membrane typologies will be examined. In all-vanadium type systems, the most common is made of Nafion.
- The membrane and electrodes are then inserted between two graphite flow plates- machined with current shunts- which direct the electrolytes into the reaction sides on the carbon paper (Refer to Figure 2.11 specifically to the element named *Bipolar plate with flow channel*). On another note, ensuring the system is sealed is crucial for it to be durable.

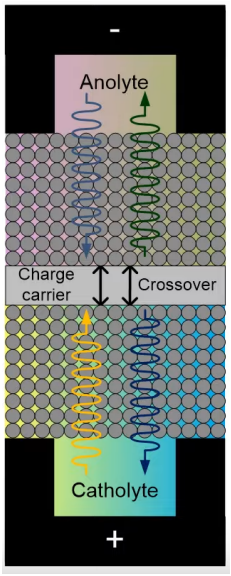

Figure 2.10 Cross section of single cell [35].

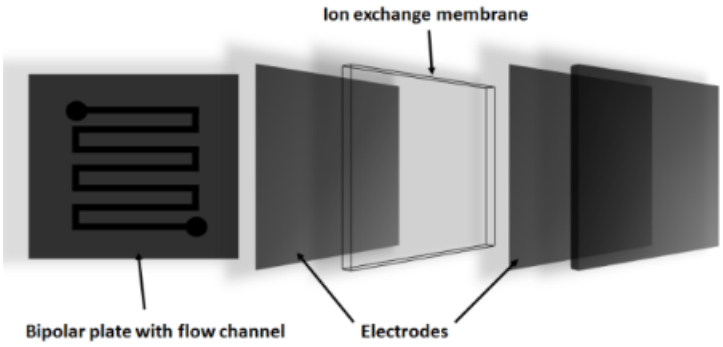

Figure 2.11 Diagram of RFB cell [72].

While the ionic equations are briefly exemplified in Figure 2.1, a clearer representation of the chemical equations is given below in Equations 2.1 and 2.2. [11]

$$VO_2{}^+ + 2H^+ + e^- \rightleftharpoons VO^{2+} + H_2O \tag{2.1}$$

$$V^{2+} \rightleftharpoons V^{3+} + e^- \tag{2.2}$$

Nonetheless, this set of equations does not reflect the full phenomena occurring in the cells. The electrolytes cannot contain solely vanadium ions at different oxidation states as this would violate the law of conservation of mass and charge balance. As can be drawn out from Figure 2.12, both anolyte and catholyte contain H^+ and SO_4^{2-} ions. These ions are however spectator ions, as they do not actively participate in the reaction and hence the reactions taking place are commonly represented through Equations 2.1 and 2.2 for simplicity. The full ionic equation remains helpful for grasping how the concentration of protons (H^+) changes and why they move across the membrane in order to maintain charge balance.

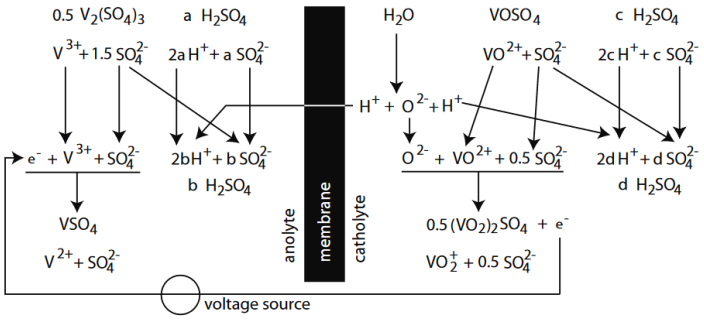

Figure 2.12 Illustration of the full ionic equations of the VRB during the charge [8].

It is derived from this thorough explanation that the operating voltage of the RFB is determined by the chemical potentials of the respective redox couples dissolved in the two half-cell electrolytes. Selection of the redox couple combinations is based on the solubility of the active ions and their redox couple potentials, which should give a good cell voltage for practical applications.[30]

As it was mentioned, in an electrochemical cell, redox reactions occur at the electrodes. The potential of each individual half-reaction is the standard electrode potential and represents the tendency of a species to undergo oxidation or reduction. [22] When the two half-cells are arranged in a stack configuration, the standard electrode potential combine to create the overall cell potential, that quantifies the driving force for the electron transfer reactions in he cell.

What is known as the voltage of a cell is directly related to the standard potential through Nerst equation[57]:

$$E_{cell} = E^0_{cell} - \frac{RT}{nF} ln(Q) \tag{2.3}$$

where:

- E_{cell} is the cell potential (voltage)
- E^0_{cell} is the standard electrode potential
- R is the gas constant ($8.314 \frac{J}{mol \cdot K}$)
- T is the temperature in Kelvin
- n is the number of electron transferred in the balanced redox equation
- F is the Faraday constant (96485 C/mol)
- $ln(Q)$ is the natural logarithm of the reaction quotient, that is the ratio of concentration of products to reactants

3 Research lines and challenges

The research topic of redox flow batteries has been a fairly inviting one over the years. With many aspects that still leave room for optimization, the variety of research lines and challenges presented is, to say the least, broad. Throughout this section, some of the prominent research lines are described in detail.

3.1 Membrane development

The membrane should be:

- A physical barrier that prevents cross-mixing of the electrolytes at the two half-cells
- However, a selective permeable that allows the transport of charge-balancing ions (such as H^+, HSO_4^- and SO_4^{2-}). This is required as portrayed in Figure 2.12 to maintain charge balance
- A chemically stable one during operation, to ensure a competitive life time
- As economical as possible

Since aqueous Redox Flow Batteries are the most commercialized ones at the moment, this section will focus on the kinds of membranes that are more apt for this use. Still studies on other membranes and diverse cases may be highlighted where relevant.

3.1.1 Membranes in aqueous RFBs batteries

Nafion, the most used material for membrane construction in VRFBs is liable for 11% of the total cost of a 1 MW/8MWh battery system. [56] It is by far the preferred membrane for an all-vanadium system.

Nafion is a fluorocarbon polymer developed by Dupont [56]. It is chemically stable but its large cost is a barrier. Nafion membranes account a high percentage of the cost- approx 40% of a cell stack. [16]

Besides this, Nafion experiences considerable crossover between the two electrolyte solutions, which is still problematic [63] as crossover leads to a reduction in coulombic efficiency.

The question may arise, hence, of why Nafion is such a popularized material for membrane construction if its crossover and cost characteristics are not exactly optimum. A fair argument is that it can withstand the acidic conditions required- $pH \leq 1$. [28]

In an all-vanadium battery, the electrolytes contain solvated vanadium ions. The ions with highest valence, refer to Figure 2.9, that is V^{5+}, require highly acidic environments for them not to potentially precipitate to oxoanions. [28]

Thus commonly electrolyte solutions for VRFBs contain up to several $molL^{-}1$ of sulfate or hydrogen sulfate ions. These severe conditions rule out many materials that are considered, for instance, for PEM fuel-cell applications.

Apart from Nafion, other anion-exchange and cation-exchange membranes were studied by the group of Skyllas-Kazacos at the University of New South Wales in Australia, especially in terms of chemical stability. Refer to [61] and [40] for further details, yet their findings will be presented and summarized below:

- **Cation-exchange membranes**. Selemion CMV and N112, where CMV proved to be the least stable one under Vanadium Redox Flow Battery conditions as oppossed to N112 that did show promisingly chemically stable.
- **Anion-exchange membranes**. New Selemion Type 2 and Selemion AMV, where Selemion type 2 showed great stability
- **Microporous membranes** Crosslinking Daramic (a microporous separator) with divinylbenzene (DVB) also showed good chemical stability

Nevertheless all membranes showed decrease in area specific resistance except N112 and New Selemion (type 2). While this effect might seem favorable, it's actually not as it was proven to be a side-effect of membrane degradation. Other membrane properties are then likely to worsen upon the evolving degradation of polymers. This effect was attributed to the oxidation of polymers due to the oxidative power of V^{5+} ions. Speaking of stability this makes N112 and New Selemion (type 2) take the lead.

Further investigations were carried out that drew light to other factors influencing membrane performance. An interesting one was the concentration of ions. However, it is seen that not always the same effect is detected as depicted from the two study cases highlighted below:

- Sukkar and Skyllas found out that for a N112E/H^{+} membrane, this one presented worse chemical stability when immersed in a 0.1M solution of V^{5+} ions than in a 1.0M solution of V^{5+} ions. This effect was attributed to a difference in swelling, when the solution was more dilute it provoked a higher degree of swelling in the membrane. This enlargement of pores allows the vanadium ions to enter into them leading to a faster degradation of the membrane [40].
- On the other hand, Soowhan Kim et al. [31] analysed the stability of sulfonated poly (sulfone) membranes (also known as S-Radel) keeping the molarity of sulfate ions constant and altering the concentration of $V5+$ ions: 0.1M and 1.7M. Refer to Figure 3.1. They found that higher concentrations of V^{5+} ions accelerated the degradation of the material.

On a note, let us take a closer look at Figure 3.1. Figure 3.1 a) is a 0.1M V^{5+} and 5.0M SO_4^{2-} stability test solution containing a N117 membrane after 74d at 40 degrees Celsius. Conversely, Figure 3.1 b) is the same stability test solution but containing a S-Radel membrane after 4 days under the same conditions. The difference in color is presumably due to the reduction of V^{5+} ions to V^{4+} ones in solution. Figures 3.1 c) and d) are pictures of the S-Radel membrane after 18 days of being soaked in 0.1M V^{5+} and 5.0M SO_4^{2-} solution and 1.7M V^{5+} and 5.0M SO_4^{2-} solution respectively. Degradation becomes more severe with increasing concentration. The severe mechanical damage is observed without obvious chemical degradation detectable by FTIR spectroscopy[31], which is why it is believed that this damage was provoked by the decrease in the weight of the polymer as a result of oxidation by the $V5+$ ions.

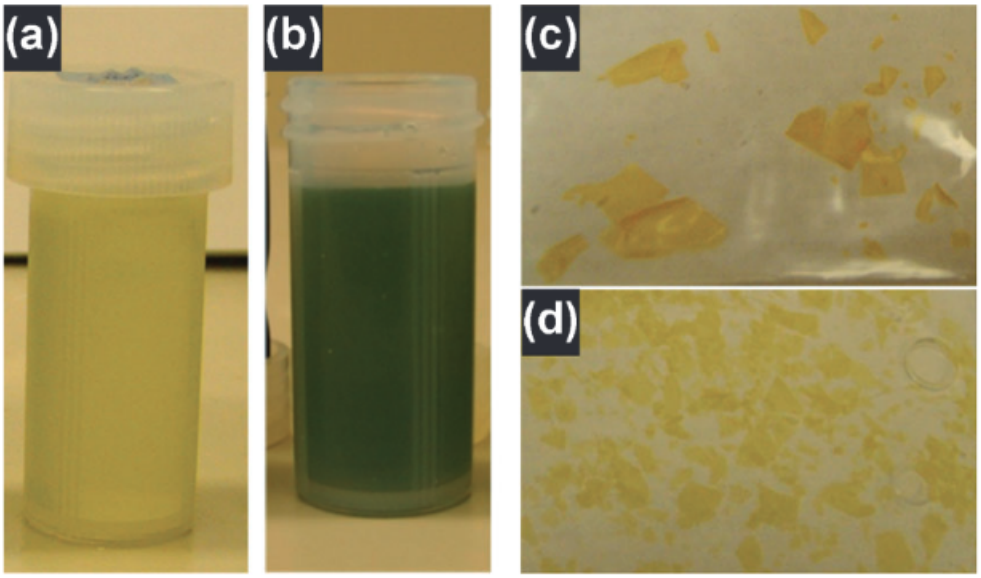

Figure 3.1 Membrane degradation results [31].

While these presented membranes have been tested in terms of stability, it is important to note that not all membranes are subjected to chemical stability tests. Henceforth, this questions the potential feasibility of multiple innovative and promising technologies for membranes. Many cycles are needed to carry out these tests and chemical stability is a vital factor when it comes to assessing this technology. Research results about stability may not receive as much attention as favorable efficiencies but it is a field that requires further investigation. Table 3.1 presents results of durability tests carrid out on a broad variety of membrane types.

Table 3.1 Durability tests for membranes [31].

Membranes	Test conditions	Results
SPEEK	Cycling (1.65/0.8 V, 50 mA cm^{-2}), 1.5 M V ion, 80 cycles	Slight efficiency loss, no holes but small dents on membrane surface
Nafion/SPEEK	Cycling (1.75/0.8 V) 1.5 M V ion, 30 cycles	Stable efficiencies
SPES	Fenton solution (3 wt% H_2O_2 + 2 ppm $FeSO_2$), 80 °C	Breakage start after 220 h, membrane disappear after 260 h
S-Radel	Cycling (1.7/0.8 V, 50 mA cm^{-2}), 2.0 M V, 45 cycles	Abrupt efficiency loss after 41 cycle Mechanical delamination
Selemion® CMV	Soaking (0.1 M V^{5+}), 60 days	Weight loss (54%), $V^{5+} \rightarrow V^{4+}$ (66%)
Selemion® AMV	Soaking (0.1 M V^{5+}), 60 days	Weight loss (6%), $V^{5+} \rightarrow V^{4+}$ (23%)
S-AMV	Soaking (0.1 M V^{5+}), 60 days	Weight loss (15%), $V^{5+} \rightarrow V^{4+}$ (30%)
	Soaking (2 M V^{5+}), 180 days	R (Ω cm^2) decrease (2.54 → 1.79)
Daramic®	Soaking (0.1 M V^{5+}), 60 days	Weight loss (23%), $V^{5+} \rightarrow V^{4+}$ (33%)
S-Daramic/DVB	Soaking (0.1 M V^{5+}), 60 days	Weight loss (18%), $V^{5+} \rightarrow V^{4+}$ (32%)
	Cycling (30 mA cm^{-2}), 2 M V ion, 1950 cycles (180 days)	R (Ω cm^2) decrease (2.52 → 2.21), diffusivity increase (53%)
Nafion 112	Soaking (0.1 M V^{5+}), 120 days	$V^{5+} \rightarrow V^{4+}$ (8%), R (Ω cm^2) decrease (57%), IEC (mmol g^{-1}) increase (1.5 → 3.6), diffusivity increase (237%)
	Soaking (2 M V^{5+}), 180 days	R (Ω cm^2) decrease (0.89 → 0.68)
	Cycling (30 mA/cm^2), 2 M V ion, 1950 cycles (180 days)	R (Ω cm^2) increase (0.89 → 1.88), diffusivity up (17%), recoverable fouling
Gore-Select L-570	Soaking (0.1 M V^{5+}), 120 days	$V^{5+} \rightarrow V^{4+}$ (2%), R (Ω cm^2) decrease (39%), IEC (mmol g^{-1}) increase (2.0 → 5.2), diffusivity up (76%)
Gore-Select L-01009	Soaking (0.1 M V^{5+}), 120 days	$V^{5+} \rightarrow V^{4+}$ (2%), R (Ω cm^2) decrease (30%), IEC (mmol g^{-1}) increase (1.1 → 2.5), diffusivity increase (7%)
Selemion® Type 3H	Soaking (0.1 M V^{5+}), 60 days	$V^{5+} \rightarrow V^{4+}$ (8%), Negligible R change, IEC (mmol g^{-1}) increase (2.0 → 3.0), negligible diffusivity change
PPR or PANI coated Nafion	Soaking (0.1 M V^{5+}), <7 days	Coating layers dissolved

S-AMV sulfonated Selemion AMV, anion type; *CMV* cation type; *S-Daramic/DVB* sulfonated divynylbenzene-crosslinked Daramic composite; *SPEEK* sulfonated poly(tetramethydiphenyl ether ether ketone), *Nafion/SPEEK* Nafion-coated sulfonated poly(ether ether ketone), *SPES* sulfonated poly(arylene ether sulfone), *PPR* polypyrrole, *PANI* polyaniline, *S-Radel* sulfonated Radel

Another factor of interest in membranes is water transport. The latter is neccessary for proton conduction as it contributes via Grotthuss mechanism along the center of the pores of the membrane. Grotthuss mechanism allows for "an intermolecular transfer of protons between water molecules in the channels penetrating the membrane" as it is the “hopping” of a hydrogen ion through permeation through the network of water molecule. [36]

Therefore, by this logic, proton conductivity would be improved by enlarging the membranes’ pore sizes. Yet this will provoke a higher degree of crossover. Investigations shall try to find them the optimum pore size as reducing them reduces both the ion transport of vanadium but also proton conduction across membrane.

Another effect to do with water transfer is that net water transfer will cause the electrolyte in one half-cell to become more concentrated and the other electrolyte more diluted in the second half-cell. This imbalance will result in a decrease in capacity and efficiency of VRFBs.

Nevertheless a study carried out by Sukkar and Skyllas in [60] shows that unless VRFBs are over-discharged, water transport within the system is not a major issue during battery operation even if net water transport imbalance occurs throughout the cycles.

Another important point on improving membranes is reducing their vanadium ion permeability. Since the diffusion of vanadium ions results in cross-mixing and hence, promotes the self-discharge of the battery it is reasonable for this parameter to be monitored. It is a standard procedure in VRFB membrane research. Normally diffusivity tests are carried out by using solutions of VOSO4, even

though it has been shown that the diffusivity of the different vanadium ions present in VRFBs varies depending on their oxidation state. [56]

Associated with this- membrane fouling- that is, vanadium ions getting trapped in the Nafion membrane. The membrane's properties can be regenerated by soaking the membrane in sulfuric acid, which removes this ion from the pores. Vijayakumar et al. recently reported an NMR spectroscopy study that focused on elucidating the interaction between N117 and the different vanadium ion species in the VRFB electrolyte solutions [70]. This finding is exemplified in Figure 3.2. Figure 3.2B is after sonication. Sonication removes any potentially surface-adsorbed vanadium species. After this process takes places two wavelength adsorption peaks become noticeable- in the range of 625 nm and 760 nm. These two ranges coincide with the values reported in literature for the absorption of $[VO(H_2O)_5]^{2+}$. In this way, study [70] concludes that membrane fouling is mostly caused by V^{4+} ions.

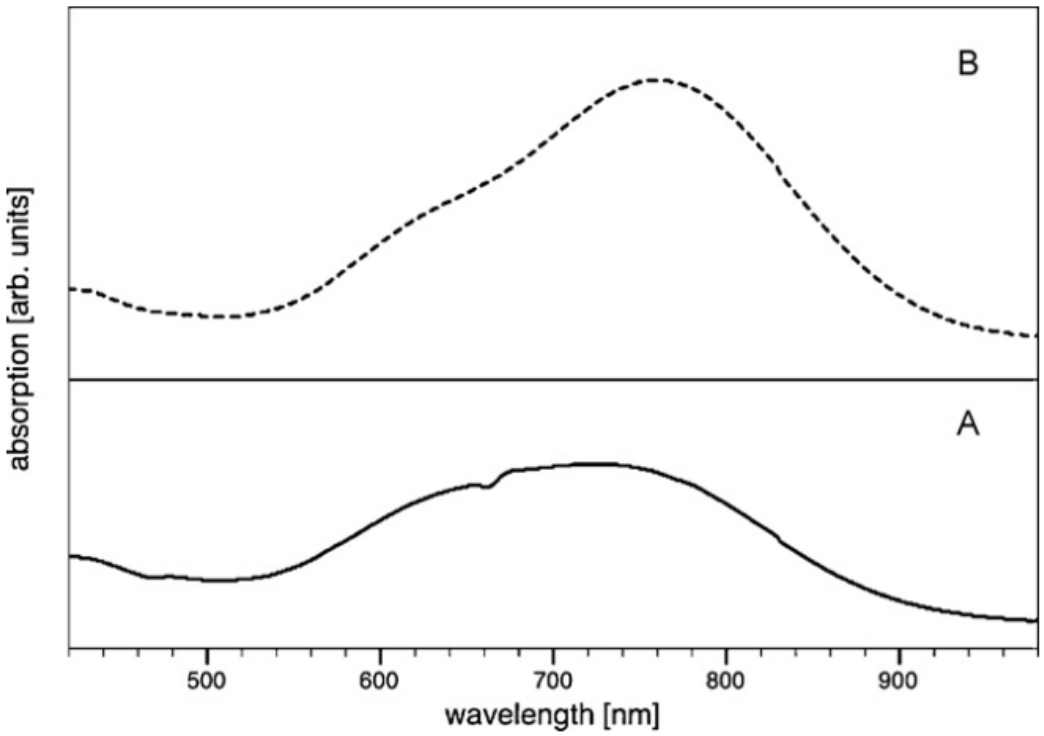

Figure 3.2 UV/Vis absorption of a Nafion membrane after cycling in a vanadium redox flow battery (A) and after sonication of the same membrane in deionized water (B). Spectrum (B) matches that of pure VO2+ solutions. [70].

On the other hand, there exist diverse papers on how Nafion sulfonic groups affect different transport properties. [55] In this study, N117 membrane was modified with polyaniline (PANI) and polypyrrole (PRP). These composite membranes showed a higher reduction of V4+ ion diffusion, interacted more strongly with sulfonic acid groups. This suggests that V^4+ ion diffusion is highly dependent on the availability of sulfonic acid group, but proton conduction is not that much. Even if PANI and PRP were intended to be used as materials for membrane development, it turned out that neither was a suitable material. PANI/N117 degraded quickly. PRP was very quickly reduced from its conductive form to its neutral structure- not useful for application.

3.1.2 Cation-exchange membrane

From now on, focus is drawn towards cation exchange membranes. In general, their main disadvantage is that they are not especially selective as to what cations cross it. Thus, the cross-mixing issue arises. [56]

Nafion and other fluorocarbon-based membranes

Nafion, a fluorocarbon polymer, consists of a hydrophobic Teflon-like backbone with hydrophilic side chains that are decorated with sulfonic acid groups. It is the most utilized material for membrane development. Still, as explored in the future economic analysis of the battery system, it turns out to be quite expensive. Most membrane development research revolves around this material.

It was found that incorporating SiO_2 particles inside the hydrophillic channels network of Nafion (see Figure 3.3) showed similar conductivity but decreased water uptake. Henceforth, less crossover was taking place as reflected in Figure 3.4. This reflected upon an energy efficiency increase from 73.8 to 79.9 %. [73]

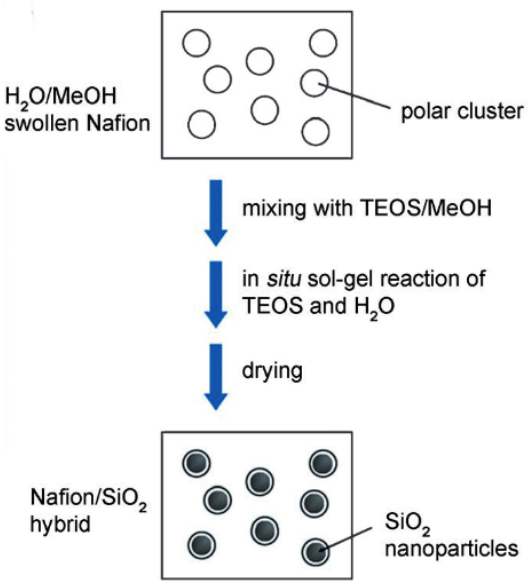

Figure 3.3 Schematic of a Nafion membrane modified with SiO_2 by sol-gel synthesis [73].

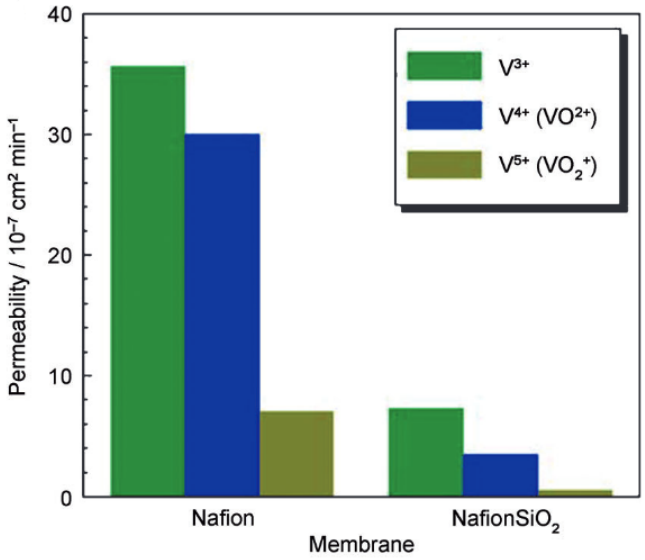

Figure 3.4 Comparison of permeabilities of different vanadium ion species through pure Nafion and Nafion/SiO_2 [73].

This finding prompted investigation of another type of compound to synthesize Nafion membranes with. A new hybrid membrane with Nafion/ORMOSIL was synthesized. This membrane showed lower water uptake, yet simultaneously, increased proton conductivity- it reported a maximum energy efficiency of 87.4%.

The same group modified the synthesis of both Nafion/SiO_2 and Nafion/ORMOSIL membranes by adding ammonia solution during the sol–gel reaction. Presumably this treatment increases the particle size of SiO_2 inside the Nafion channels. The observed V^{4+} ion diffusion through their membranes is about half that reported by previous studies. [54]

Additionally, other fluorinated polymers around 10-15 years ago were investigated, such as PVDF-g-PSSA-co-PMAc but no further results have been reported. [56]

Hydrocarbon-based membranes

Other hydrocarbon-based membranes were investigated due to the interest of them being more cost-effective than Nafion ones. However, most of them were to be found unstable in acidic environment. [56]

Nevertheless, in 1996, Hwang and Ohya [26] tested out photochemically chloro-sulfonated low-density polyethylene (PE) membranes and asymmetric membranes (PE+chemically bonded to porous polyolefin films containing silica particles). They were crosslinked and sulfonated to different degrees. Authors proposed that asymmetric membranes would have very high coulombic efficiencies (low diffusion coefficient for most vanadium ion species and an area specific resistance comparable to N117). However, this proposal was not demonstrated in any publication afterwards. [26] [56]

In an effort to find an alternative to Nafion membranes, SPEEK- sulfonated poly(ether ether ketone) membranes came across as another possible viable option. Luo et al. [37] findings are summarized in Table 3.2.

Table 3.2 Comparison of parameters for N117, Nafion/SPEEK, and SPEEK membranes [37].

Parameter	N117	Nafion/SPEEK	SPEEK
Thickness [mm]	175	100	100
IEC [mmol/g]	0.91	1.67	1.8
Area specific resistance [W/cm^2]	1.06	1.61	1.27
Permeability of V^{4+} (10^{-7} cm^2/min)	36.55	1.93	2.43
Coulombic efficiency [%][a]	93.8	97.0	97.1
Voltage efficiency [%][a]	90.7	85.3	87.3
Energy efficiency [%][a]	85.0	83.4	84.8

[a] Values for efficiency parameters are given for comparison purposes.

Since SPEEK and Nafion/SPEEK are thinner than N117, this makes the comparison difficult:

- area specific resistance of SPEEK is a lot higher yet the membrane is thinner, assigning a disadvantage to SPEEK
- The voltage efficiency drops considerably as a result on Nafion/SPEEK
- Coulombic efficiency is higher (IEC is higher and decreased ion V^{4+} despite being thinner)

An important point to make SPEEK is not very stable in the oxidizing environment of V^{5+} positive half cell [37]. Coating it with Nafion would solve this issue.

In the author's opinion, [37], the lower cost and compromise between its capabilities puts the Nafion/SPEEK membrane at an advantage. Overall energy efficiency is still worse. However long-term stability may be problematic because of the layered structure of the composite membrane: interfacial delamination might occur after prolonged exposure to the electrolytes coupled with mechanical stress during operation. [37] [56]

Unlike what occurred to fluorinated polymers, research on SPEEK membranes continued. Mai et Al. [38] tested SPEEK membranes to different degrees of sulfonation .They found out that as sulfonation increases, diffusivity of V^{4+} increases. [38]

The V^{4+} ion permeability was still lower than through N115, which is thicker (127 vs 85 micrometers). Refer to Figure 3.5- this figure puts forward how the selectivity is greater in SPEEK60 than in Nafion115. SPEEK 40 has sulfonation degree of 0.73 and yields the highest coulombic efficiency of the three.It overall yields a higher energy efficiency even if voltage efficiency is lower. 87.5% compared to 84.7% N115.[38]

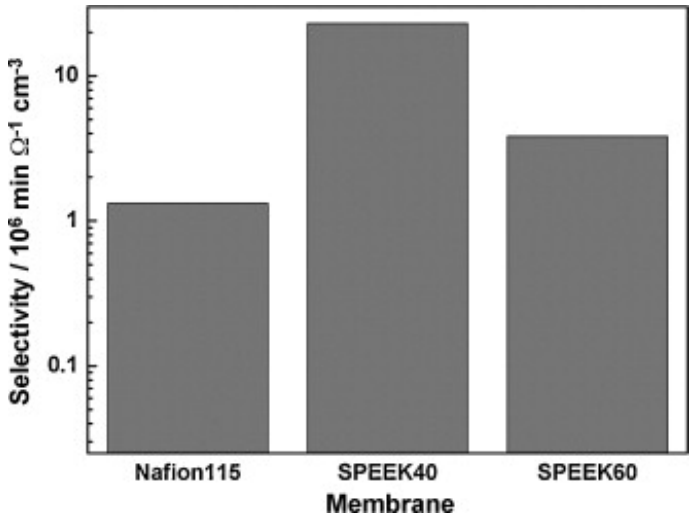

Figure 3.5 Selectivity in permeability of V^{4+} ions and protons [38].

Stability is very promising in this experiment as well, as can be depicted from Figure **??**.

Chen et Al. [12] synthesized other types are SPTK (Sulfonated poly arylene thioether ketone) and SPTKK (arylene thioether ketone ketone) membranes, which showed high coulombic efficiency. See Table 3.3.

Table 3.3 Proton conductivity and VO_{2+} permeability of SPTK, SPTKK, and Nafion 117 membranes at room temperature [12].

Membrane	Proton Conductivity ($\times 10^{-2}$ S cm^{-1})	VO^{2+} Permeability (m^2 s^{-1})
SPTK	1.05	1.2×10^{-13}
SPTKK	1.36	3.1×10^{-13}
Nafion 117	2.03	4.9×10^{-12}

3.1.3 Anion-exchange membranes

One of the membrane types left to discuss is anion-exchange membranes. They could be promising technology as they would circumvent cross-mixing of all vanadium cations. In this way, efficiencies close to 100% could be achieved.

Nevertheless, since it is an anion-exchange membrane, as well as reducing permeation of vanadium ions, it also hinders the conduction of protons. This latter effect sacrifices voltage efficiency. [56]

Selemion AMV and New Selemion Type 2 were investigated through sulfonation. The effect it had was reduction of water transport, and hence, reduced capacity loss as an advantage. However, it is already known that energy efficiency is also reduced due to this effect. [39]

Interesting studies on custom-made poly ether sulfone [75], poly(ether sulfone ketone) [27] were conducted. About the poly(ether sulfone ketone) membrane, compared to N117 membrane it was reported that [27]:

- Similar chemical stability in solutions with V^{5+} ions
- Higher energy efficiency (88.3 vs. 82.9%) due to:
  - Similar voltage efficiencies (91.6 vs. 90.6% for N117)

– Increased coulombic efficiency (96.4% vs. 91.5% for N117)

Note that if the energy efficiency is higher, maintaining the voltage efficiencies at a similar or even greater level, it implies that the membrane is more **selective**.

On the contrary, the poly(ether sulfone) membrane did report a lower voltage efficiency, even if the overall energy efficiency was higher due to a greatly increased coulombic efficiency- the membrane was thus less selective. It reduced the permeation of vanadium ions but also limited proton conduction. Increased amounts of amine functional groups resulted in more enhanced ion exchange capabilities. [75]

Also chemical stability and higher water transport are additional issues. They are being studied and this research may lead to the construction of more efficient and complex hybrid membranes leading to the mitigation of these problems.

3.1.4 Amphoteric ion-exchange membranes

An interesting field of study is that of amphoteric membranes. They consist of membranes with different types of functional groups that may aid or prevent ion transport-cationic and anionic. For example, in [74], varying layers of polyanion (PPDA) and polycation (PSS) were included to the surface of Nafion N117 membranes. The nomenclature followed is , where n is the number of multilayers. This model was tested for n=3,5 and 7. Refer to Figure 3.6.

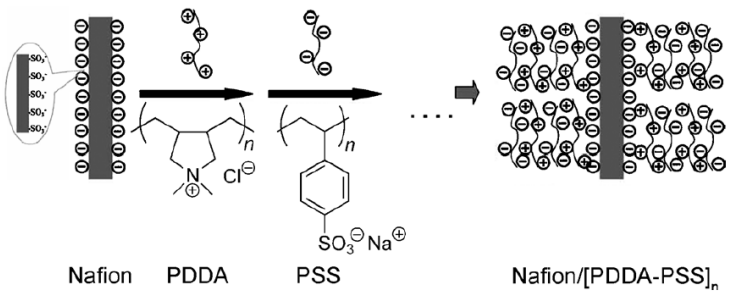

Figure 3.6 Layer by layer self-assembly of Nafion-$[PDDA - PSS]_n$ [74].

This configuration embodied reduced vanadium ion permeability (by 6-10 times less when compared to pure Nafion). Moreover, proton conductivity was slightly lower than for pure Nafion- around $50 mS cm^{-1}$, for n=3,5,7. [74]

This configuration was also stable for 50 cycles, which is promising for a first design. In terms of efficiencies, higher values were achieved when compared to N117 membrane' efficiencies. [74]

3.1.5 Nonionic separators

On another note, nonionic separators have been evaluated for use in redox flow batteries. Interest is drawn towards them because of their cheap price and the fact that they are already in use in other battery types (such as lithium ion or nickel cadmium batteries). For this application, pore size was found to be too big. As a result, the big degree of vanadium ion permeability was unacceptable. [56]

Nevertheless, inserting modifications that reduce the pore size of this material makes it apt to use it as a redox flow battery membrane. For example, Daramic/Amberlite400CG later crosslinked with DVB is a composite membrane that has yielded an energy efficiency of 83%with a coulombic efficiency of 95% and a voltage efficiency of 85%. [40]

A charge/discharge cycling test for 8000 h (1650cycles) was performed on another Daramic/Amberlite 400CG/DVB composite membrane; this membrane had an energy efficiency of 72.7% and showed excellent stability over the whole cycling time. [13]

On another note, membrane swelling is a clear obstacle to elaborate commercially feasible membranes. [56]. So is the need for materials that resist a very acidic environment, since otherwise V^{5+} ions cannot be kept and will eventually undergo precipitation to oxoanions.

3.1.6 Membrane-less

Apart from all of these studies, some scientists have pursued the idea of going membrane-less- Refer to Figure 3.7. [9]

However, aqueous electrolytes are limited for output potential, namely water electrolysis happens at 1.23 V in standard condition, which limits the energy density.[9]

Introducing inorganic nanoparticles has been proved effective to modify the porous membranes.[9]

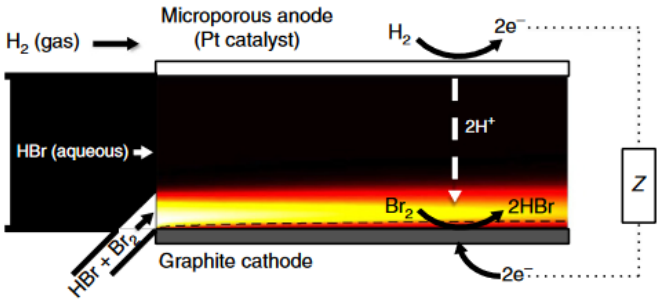

Figure 3.7 Schematic of reactant flow within the HBLFB [9].

3.2 Electrolyte Chemistry and Optimization

Different redox couples have been tested out over time searching for the most efficient chemistry. Most industrialized redox flow batteries are vanadium redox flow batteries (VRFBs) and zinc-bromine flow battery (ZBFBs). Nevertheless more species have been investigated seeking the best candidates that will provide higher energy efficiency, that is, high values for both; coulombic and voltage efficiencies. This section will highlight some of them.

3.2.1 Simple inorganic ions

All-vanadium redox flow battery

First proposed by Skyllas-Kazacos, it only employs vanadium in both catholyte and anolyte so contamination due to crossover is not an obstacle. Therefore, a long system life can be achieved-approx 5-20 years. [47] Fast electrochemical kinetics with a short response time is a plus. [53]

As disadvantages, it is worth noting that:

- Strong corrosive strength
- Less energy density than lithium-ion batteries, for example

Iron-chromium

This configuration was primarily developed by NASA [17], delivering a cell voltage of 1.18V. As per the reactions Equation 3.1 shows the cathodic one and Equation 3.2 shows the anodic one.

$$Fe^{3+} + e^- \longleftrightarrow Fe^{2+} \tag{3.1}$$

$$Cr^{2+} - e^- \longleftrightarrow Fe^{3+} \tag{3.2}$$

While the cathodic reaction shows good reversibility and fast kinetics, the chromium reaction at the anode presents a bottleneck: it requires an elevated operation temperature and its low redox potential invites for H_2 evolution to happen. [47]

Zinc-bromine flow battery ZBFB

It is another successful system, that works according to the following equations:

$$Br_2 + 2e^- \longleftrightarrow 2Br^- \tag{3.3}$$

$$Zn - 2e^- \longleftrightarrow Zn^{2+} \tag{3.4}$$

Equation 3.3 is the cathodic equation and 3.4 is the anodic equation. It is a hybrid flow battery [53]. This means that one or more of the active components are "deposited on the electrode as a solid layer"[46]. Refer to Figure 3.8, where deposition becomes visible at the anode.

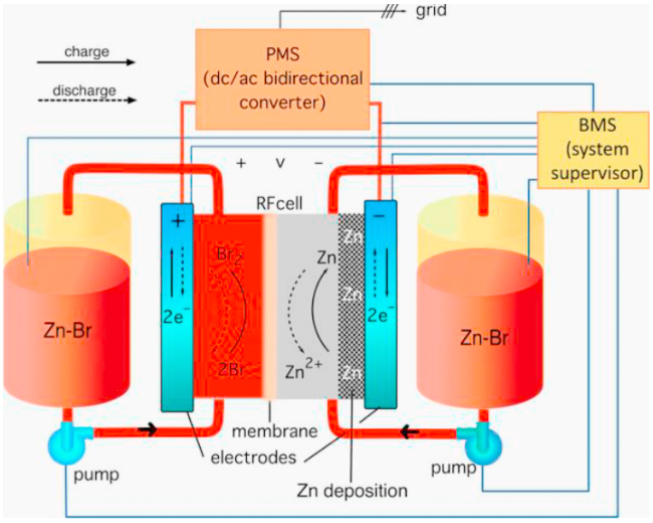

Figure 3.8 Scheme of a kW-class hybrid Zn-Br system [53].

In this process of dissolving and depositing, dendrite can grow and after a large number of cycles which may cause channel blockage, and hence cell failure. [53] In order to palliate this side-effect, the battery must be fully discharged every few days. This represents a clear downfall.

Vanadium-oxygen redox flow battery

It follows these reactions at the positive electrode and negative electrode respectively, giving a standard cell voltage of 1.49V:

$$O_2 + 4e^- + 4H^+ \longleftrightarrow 2H_2O \tag{3.5}$$

$$V^{2+} \longleftrightarrow V^{3+} + e^- \tag{3.6}$$

As advantages:

- Increased energy density
- Less quantity of vanadium, which is expensive, is required

However,

- The positive electrode's reaction shows a low degree of reversibility, this could be fixed by adding an electrolyzer provided with special catalysts[53]
- It has only been tested at a small scale [53]
- Long term stability is a challenge[53]

3.2.2 Aqueous organic redox flow batteries (AORFBs)

Pursuing savings in terms of cost, it becomes clear that using materials that are ubiquitous (C,H,O,N,S) for electrolytes is a reasonable option. Research is however focused on anolyte design and there is little development on catholytes. [53]

Carbonyl based electrolytes

Largely explored, no candidate has been considered a viable solution. For instance, Aziz et al. [25] used anthraquinones as anolytes in acid media and chose as catholyte one with bromine. This AQDS/Br flow battery delivered 0.8V, which is relatively low when compared to other flow batteries, yet reached a high level of power density, greater than $0.6 W cm^{-2}$. It experimented high crossover rates, decreasing coulombic efficiency. In subsequent developments [24], through membrane modification, they managed to lessen this crossover phenomenon, improving the coulombic efficiency by 3.35 percentage points. It showed good stability for 750 cycles. [53]

Quinoxaline based electrolytes

Regarding quinoxaline based electrolytes, further experiments require examining long term stability, as the only experiments that have been carried out with long-cycling are done in a short period of time. Nevertheless, some findings are promising. For instance, Wang et al. [23] developed a system with $DHPS/K_4[Fe(CN)_6]$ with the following features:

- 1.4V cell voltage
- Energy efficiency greater than 75%.
- Capacity retention of 99.98%, that is almost no capacity degradation, over 500 cycles
- High capacity achieved $67 Ah L^{-1}$

3.2.3 Metal-solution based redox pairs flow batteries

Appealing due to its low raw cost, like Zn, Fe, Cu, or PB, can be chosen as anode. These materials, especially zinc, iron and copper, are eco-friendly and easily recyclable. On the contrary, side-reactions may occur like hydrogen evolution reaction (HER) and dendrite formation. [53] As an illustration Zn based flow batteries are briefly commented below:

Zn based flow batteries

Reactions that occur at the anode for this type of batteries are detailed below:

$$Zn \longleftrightarrow Zn^{2+} + 2e^{-} \tag{3.7}$$

$$Zn + 4OH^{-} \longleftrightarrow [Zn(OH)_4]^{2-} + 2e^{-} \tag{3.8}$$

At the positive electrode, Nickel is an abundant pick:

$$2NiOOH + H_2O + 2e^{-} \longleftrightarrow 2Ni(OH)_2 + 2OH^{-} \tag{3.9}$$

As advantages, they present:

- Low cost
- Fast electrode reaction
- High solubility of Zn(II) ions
- For the Zn/Ni a high cell voltage of 1.73V is exhibited

Some of the downfalls that they exhibit are mentioned below:

- Less durable due to uneven depostion at the electrode during battery charging
- Dendritic deposits that lead to cell failure
- HER occurs, diminishing the efficiency

4 Case study: Economic feasibility

This chapter will take an approach on the economic feasibility of a Vanadium Redox Flow Battery in Spain. To do so, there are two main tasks that precede this process in the following order:

1. Selection of a cost analysis methodology
2. Selection of a viable battery model to apply such analysis

Since the information available on different battery systems investigated so far is not especially abundant, there is a strong relationship between the aforementioned steps.

Diverse cost analysis examples were evaluated. For instance, [29] deals with the comparison of a redox flow battery against other forms, such as fossil fuel-based spinning reserve to review the viabiliy of this technology. On the other hand, Zhang [78] studies the sensibility of different factors (such as membrane cost or current density) on an All-Vanadium Redox-Flow Battery's capital cost.

After having examined some of them it is worth pointing out that it is not at all trivial to implement these methodologies, as their intrinsic complexity make them rely on not readily available nor estimable data. However, the observations and results obtained by them will be discussed later on as part of this work.

Finally the selected methodology is briefly described in [42] and exemplified in [44], [59], [5] and [43], among others. It is a methodology inspired from one developed by Douglas, a step-by-step hierarchical process often used in chemical engineering classes proceeding through decision levels where more details are added to the flow sheet at each step or level of the design procedure [14] [42].

Nevertheless at some points in the methodology it becomes necessary to make assumptions as the required data is not readily available.

4.1 Electrical network parameters in Spain

To study the viability of the system and analyse whether it is or is not economically profitable, the reasoning will be to calculate the difference between income produced and cost incurred. Some main assumptions are made:

- The battery will charge at all times at **off-peak** tariffs, retrieving the energy from the network
- The battery will discharge at all times at **peak** tariffs, selling the energy at such electricity price

- The battery will have continuous cycles of charging and discharging and will work non-stop 24 hours a day, 365 days a year

Needless to say these premises are not realistic since it would imply that the charge and discharge cycles of the battery are always in sync with the hours providing off-peak electricity prices and peak electricity prices respectively. Since the battery never stops working, this will never happen, but it is assumed for simplicity. An availability factor (ranging from 0 to 100 %) could be taken into account if the study results were not clearly conclusive.

That said, next step is to establish the cost of electricity at peak (*punta*) and off-peak (*valle*) hours to be used in the study, which is not fixed in Spain. The gap between these two favours the study, as more revenue is produced.

The most familiar tariff is Evolution of Voluntary Price for Small Consumers (PVPC) Tariff 2.0TD. It distinguishes between three different price ranges [45]:

- Punta. Peak hours
- Llano. Valley time band
- Valle. Off-peak hours

Its evolution starting from 2022 until may 2023 is graphed below as per the data in [45] .

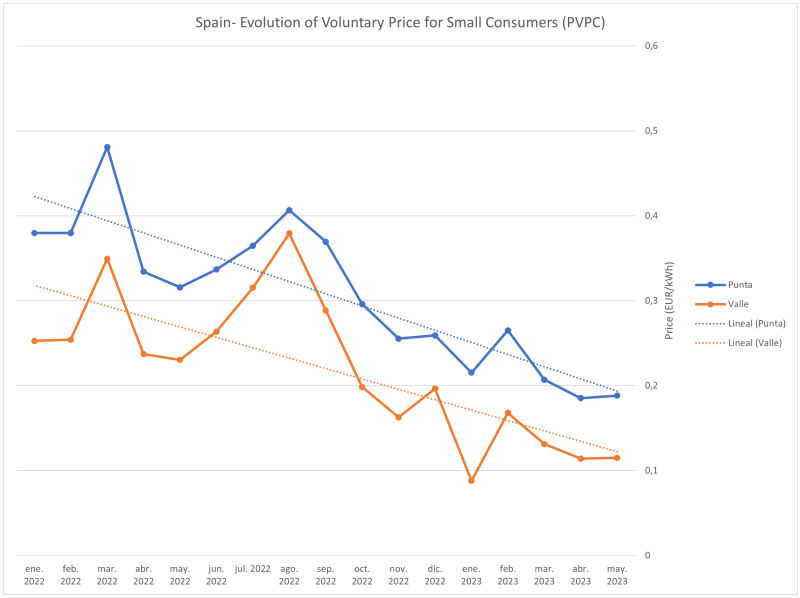

Figure 4.1 Tariff 2.0 TD, Evolution in time [45].

An important point to note is that from this graph, for instance, the following prices could be extrapolated:

- 0.2 EUR/kWh for peak hours
- 0.1 EUR/kWh for off-peak hours

Still, already in Tariff 2.0 TD, it becomes notable that this data is highly dependent on the moment in time the data is gathered at. Apart from this it is worth pointing out it would not be entirely suitable to take these prices as a whole in the approximation of selling the energy. Refer to Figure 4.2, it infers that a high percentage of the price paid for being connected to the network, around 65 % is attributable to taxes and electricity tolls, instead of the energy being consumed itself.

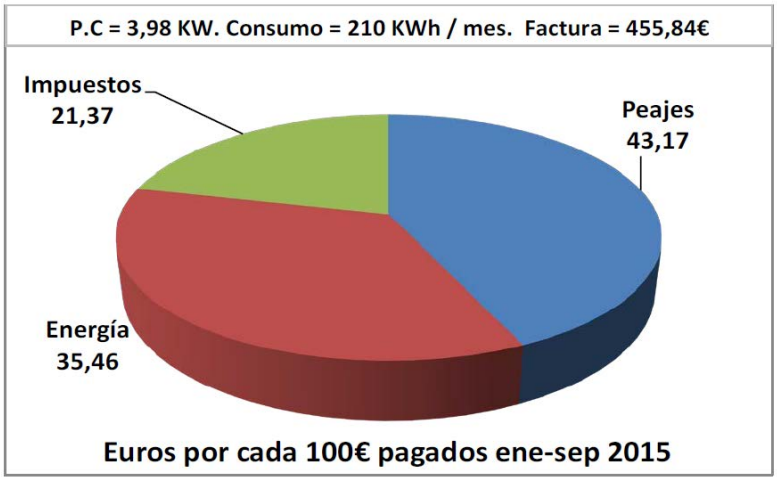

Figure 4.2 Percentages of prices of energy [19].

In any case, PVPC prices and Tariff 2.0 applies to users of low voltage electrical networks with a hired power less than or equal to 15 kW. [3] As will be further detailed in Section 4.2, the considered battery system is 450 kW. Hence keeping in mind the already established assumptions, reducing the number of assumptions made will provide more veracious results. Therefore, a broader investigation on the tariffs according to power requirements is carried out.

As it as published in the *Boletín Internacional del Estado (BOE)* [2], electricity consumers in Spain are divided into *grupos tarifarios*, defined as "grouping of supplies with the same connection characteristics at the same tariff voltage level and with same hourly discrimination" [2] Find below in Table 4.1 a summary of the different voltage levels since 2021 in Spain:

Table 4.1 Definition of transport and distribution tolls in Spain.

Type of supply	Characteristics	Applicable tariff
Low voltage	$\leq$ 15 kW	2.0 TD
Low voltage	$\geq$ 15 kW	3.0 TD
High voltage	1 kV $\leq$ V $\leq$ 30 kV	6.1 TD
High voltage	30 kV $\leq$ V $\leq$ 72,5 kV	6.2 TD
High voltage	72,5 kV $\leq$ V $\leq$ 145 kV	6.3 TD
High voltage	$\geq$ 145 kV	6.4 TD

As it can be depicted, the applicable tariff to be considered is 6.1 TD. It must be noted than even if the system is 450 V and not 1 kV, the limiting factor is the requirement to be connected to a high voltage network due to the power conditions of the system. In this way, step-down inverters and converters will allow for the connection.

A few comments must be made on 6.1 TD tariff. This tariff is applicable to big industries who require a high voltage supply for their infrastructure and associated devices. This tariff establishes six periods of consumption (P1, P2, P3, P4, P5, P6) and six periods of power, in such a way that each one has a different price. Nevertheless, to simplify the calculations, again, the cheapest price (analogously off-peak hours) will be assumed for charging and the most expensive one (analogously peak hours) for discharging the battery system. Refer to the following Figure extracted from Endesa-Tarifa Óptima 6.1 TD, aplicable in 2023 up to 450 kW (the whole document is attached in Appendix A

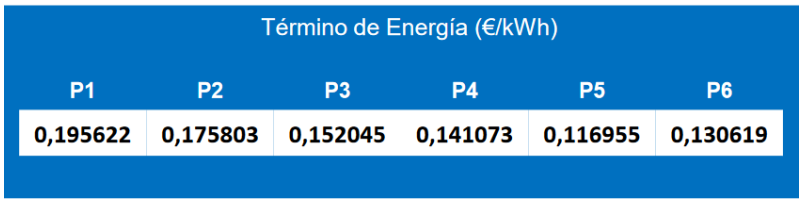

Término de Energía (€/kWh)					
P1	P2	P3	P4	P5	P6
0,195622	0,175803	0,152045	0,141073	0,116955	0,130619

Figure 4.3 Tariff 6.1 TD [4].

Hereinafter the following approximate values are used after considering the above inputs:

- 0.2 EUR/kWh for peak hours
- 0.1 EUR/kWh for off-peak hours

These two values have been estimated from data in P1 and P5.

4.2 Main characteristics of system proposed

The goal of this study is to examine the economical feasibility of a realistic system in a lifelike environment. The environment has already been picked (Spain and its tariffs) and now it's time to define the system.

The purpose of a realistic system further complicates the study, since not that many big-scale industrial systems have been implemented. Research carried out reaches the conclusions that:

- Many investigations (e.g. membrane, ions selection, electrode selection) have been carried out at a small scale
- Regarding the few industrial systems, two main issues arise:
  - Detailed information on the system is not readily available, which is required to carry out the study
  - Not many systems have been checked in terms of stability. This point turns out to be crucial as it is only a long-term analysis that can ensure the economic feasibility of the solution

Considering these factors, finally the approach is to pick a real-life system, whose stability has been already proven over a substantial period of time. Obviously the available information and data must be as much as possible, so that the conclusions drawn are mostly based on facts and the system's characteristics as opposed to assumptions.

The chosen system is a 450-kW system which was installed in 1996 in Tatsumi Substation of the Kansai Electric Power Co. Ltd. Refer to [66] and [65]. This battery is an all-vanadium one. A block diagram of the system is shown below in Figure 4.4

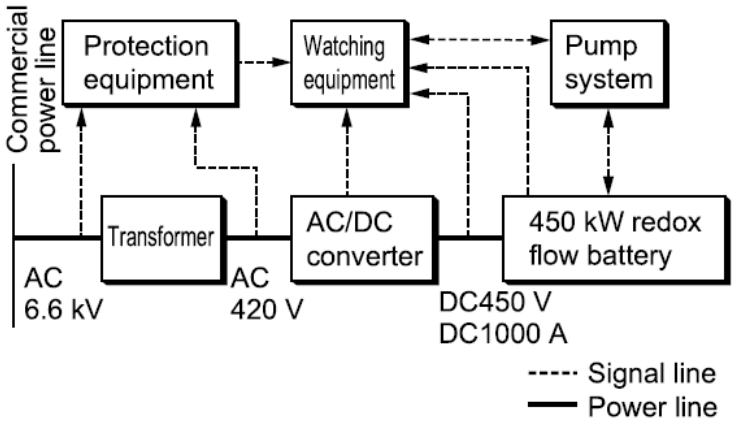

Figure 4.4 450-kW system concerned figure [66].

It is noticeable there are additional systems that support a safe connection to the network, a transformer and AC/DC converter- joint by a power line. Signal lines are added to account for the pump system, protection equipment and watching equipment. The analysis presented in this Section will estimate the costs of all the subsystems joint by power lines as well as the pump system.

The readily available data is presented and calculated when not directly given through the article. The 450kW battery is made from battery cell stacks of 18.8 kW each, with the following characteristics:

Table 4.2 20-kW battery system specification [66].

DC output	18.8 kW
DC voltage	75.2 V
DC current	250 A
Area of electrode	5000 cm^2
Cell stack	60 cells (series)
Electrolyte	Vanadium 1M Sulfuric acid solution

Therefore, the battery system is built by piling up stacks of this sort in series and parallel. Specifically, one module is achieved by piling up cell stacks in a 4P x 2S configuration, meaning that one module obeys:

$$V_{DC} = 2 \times 75.2V = 150.4V \tag{4.1}$$

$$I_{DC} = 4 \times 250A = 1000A \tag{4.2}$$

In turn, modules are piled up in series of three, so that:

$$V_{DC} = 3 \times 150.4V = 451.2V \approx 450V \tag{4.3}$$

These calculations exemplify the fact that piling up cell stacks in series increases the voltage, whereas piling them up in parallel increases the current. Thus, the readily available specifications of the whole system are:

Table 4.3 450-kW battery system specification.

DC output	450 kW
Battery capacity	900 kWh (450 kW x 2 hours)
DC voltage	450 V (av.)
DC current	1000 A (av.)
Cell module	1 module: Cell stack 4P x 2S Series of 3 modules
Electrolyte	Vanadium 1M Sulfuric acid solution
AC/DC converter	PWM control

The current density of current collectors is $50\frac{mA}{cm^2}$ [66].

On another note, as mentioned before, the stability of the system is mandatory. The 20-kW battery system cycle life test presents the following results in Figure 4.5:

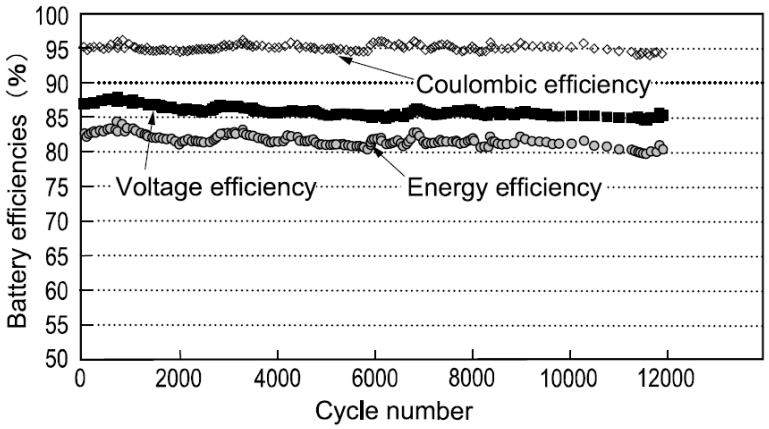

Figure 4.5 20-kW battery system cycle life test [66].

There is no substantial downfall through 12000 cycles of the three key efficiencies (coulombic, voltage, energy). This test was carried out in half an hour cycles. This proves the stability of a single stack. The efficiencies of the 450-kW battery system were estimated to be:

Table 4.4 Result of 450-kW battery system Charge/Discharge test.

Test items	Means of operation	Constant current
	Charge/Discharge current	1000 A
	Coulombic efficiency	96.7 %
Battery efficiency	Voltage efficiency	85.1%
	Energy efficiency	82.3%

4.3 Methodology

4.3.1 Summary

The methodology proposed is developed by Moore et Al. [42] and inspired by a hierarchical step procedure devised by Douglas [14]. Douglas in [14] proposes a methodology of several steps that include heuristics for the design of a chemical system. This method is designed in an additive

manner, so that if economic infeasibility of the system is detected in one of steps (so called levels), the procedure is stopped and the conclusion of infeasibility reached. The same philosophy is used in Moore's approach. Since the costs can be classified into three areas [42]:

- Costs that scale in proportion to the power capacity
- Costs that scale in proportion to the energy capacity
- Costs that do not scale with size (the control system and balance of plant)

The method proposed by Moore studies six different levels [42]:

- Level 1. Input information for the VRB
- Level 2. Input-output analysis
- Level 3. Power capacity considerations
- Level 4. Energy capacity considerations
- Level 5. Control system and balance of plant
- Level 6. Total capital investment estimate

4.3.2 Level 1: Input information for the VRB

4.3.3 Level 2: Input- Output Analysis

Level two aims to obtain the maximum economic potential of the VRB. The philosophy behind is for it to be the difference between the product value and the raw material cost, not taking into account processing costs. The equation that embodies this concept is given below:

$$EP_2 = (E_D \times \frac{€}{kWh_D} - E_c \times \frac{€}{kWh_c}) \times \frac{cycles}{year} \tag{4.4}$$

E_c and E_D are defined by:

$$E_c = \frac{E_{sc}}{\xi_c} \tag{4.5}$$

$$E_d = E_{sc} \times \xi_D \tag{4.6}$$

The number of cycles per year is the variable to be plotted in the x-axis, while the economic potential will be in the y-axis.

For simplicity, it is assumed that $\xi_c = \xi_d$. As the cycle efficiency is, as its name implies, the efficiency of the entire cycle, it is estimated to be the product of te following efficiencies:

- Energy efficiency
- Transformer Efficiency
- PCS efficiency

The energy efficiency is retrieved from the experiments carried out in the actual system and it is 0.823. Refer to Table 4.4. On the other hand, the transformer and PCS efficiencies are estimated to be 0.995 and 0.97 respectively as taken from [44]. In this way:

$$\xi_c = \xi_D = 0.891 \tag{4.7}$$

since it is assumed that:

$$\xi_c \times \xi_D = \eta_{energy} \times \eta_{trans} \times \eta_{PCS} \tag{4.8}$$

The battery capacity is taken to be 900 kWh as indicated in Table 4.3.
Also, it is induced from Section 4.1 that:

$$\frac{€}{kWh_D} = 0.2 \tag{4.9}$$

$$\frac{€}{kWh_C} = 0.1 \tag{4.10}$$

Therefore, the following curve for the Level 2 Economic Potential (EP2) is obtained.

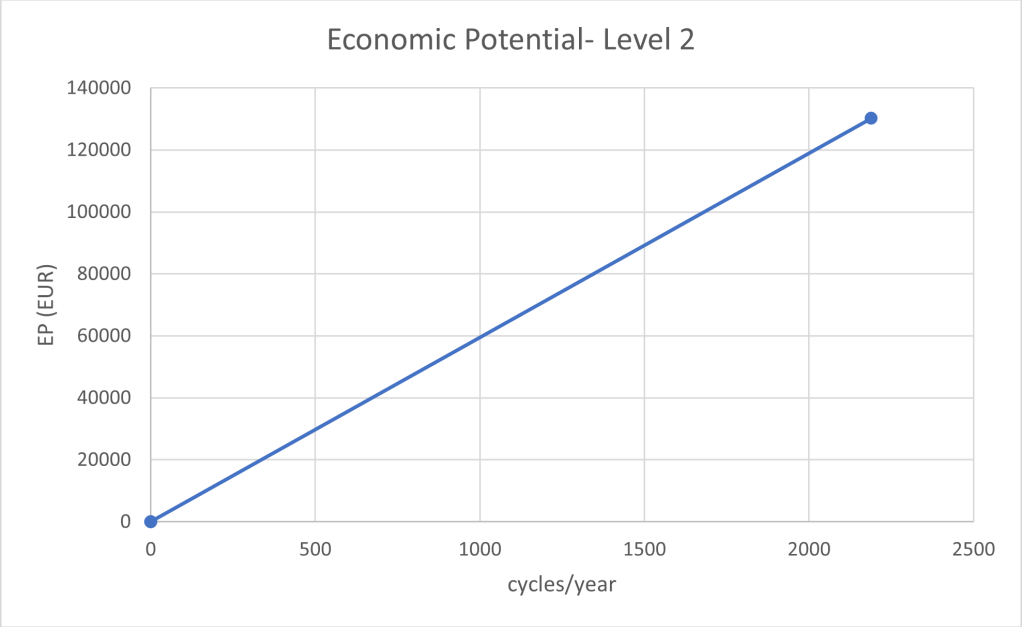

Figure 4.6 Level 2 Economic Potential.

A cycle is considered when both charging and discharging have occurred. Since it takes 2 hours for its mid-cycle to complete, it is estimated that the maximum achievable economic potential is given when 6 cycles occur per day, that is, the battery is always charging and discharging-never stops working. In a year this is **2190 cycles**. Following the equation that the Figure 4.6 obeys, the maximum achievable economic potential is 130149 euros, that is approximately **130k€**.

4.3.4 Level 3: Power Capacity Considerations

The next step to follow is accounting for the costs of the power capacity considerations. The materials and equipment that will be taken into account, are therefore:

- The heat exchangers
- The pumps
- The cells themselves
- The PCS that converts electricity in AC form (as it's given from the network) to DC, so as to charge the battery, and viceversa, when discharging takes place

Heat exchangers

To start with, let us examine whether heat exchangers are required in this design. The amount of heat that may increase the system's temperature, and thus, need dissipation is the energy lost due to inefficiencies. This energy is calculated as follows:

$$q_C = \frac{P}{\xi_C} \times (1 - \xi_C) \tag{4.11}$$

$$q_D = P \times (1 - \xi_D) \tag{4.12}$$

It turns out to be logical that $q_C \geq q_D$, as more heat is dissipated during charging. In this case:

$$q_C = 26.68kW \tag{4.13}$$

$$q_D = 25.18kW \tag{4.14}$$

One assumption made within this procedure is that this heat is shared equitatively between the anode and cathode solution with the temperature change of the vanadium ion solutions dependent on the flow rate of the vanadium solution though the stack. [42] To calculate this flow rate, the moles of vanadium ions oxidized per second is divided by the molarity of the vanadium ions in the solution:

$$F_M = \frac{I_s \times N_c \times N_s}{F \times C_v} \tag{4.15}$$

In Equation 4.15 [42]:

- F_M stands for the minimum flow rate assuming all flowing vanadium ions are oxidized, that is full conversion in l/s
- I_S stands for the current through a stack in A
- N_C stands for the number of cells per stack
- N_S stands for the number of stacks in the battery
- F stands for Faraday's constant in C/mol
- C_V stands for the concentration of vanadium ions in mol/L

Breaking Equation down:

- $I_S = 250A$ as shown in Table 4.2
- $N_C = 60$ as shown in Table 4.2
- $N_S = 24$ since there is a total of twenty-four modules in the 3 x (4P x 2S) configuration
- C_V is 1M as exemplified in article [66]

Henceforth, $F_M = 3.73\frac{L}{s}$

However, not all vanadium ions that flow through the cells are oxidized. Transport loss is a phenomenon that occurs in RFBs and it is intrinsically associated with the incomplete conversion of all posible V ions flowing through the battery. Being aware of this effect, it will be assumed that the minimum flow rate represents 10% of the greater bulk rate, so that:

$$F_A = \frac{F_M}{X_{V,P}} \tag{4.16}$$

, where F_A represents the actual flow rate of vanadium ion solution and $X_{V,P}$ the fraction of vanadium ions converted per pass.

Once the flow rate has been obtained, the change in temperature of the solution is calculated by [42]:

$$\Delta T = \frac{q}{2 \times C_p \times F_A} \tag{4.17}$$

Note that here in Equation 4.17 the specific heat capacity of the electrolyte is required.

It is retrieved to be $4.2 \frac{J}{gK}$ from [50]. Refer to Table 4.5 in [50], where the heat capacity of commercial electrolyte (CE) is given. This same article establishes that the specific heat capacity is practically insensitive to the molarity of the vanadium solution. Additionally, in other studies such as [59] this same value is used as reference for the specific heat capacity.

Table 4.5 Composition and thermodynamic properties for commercial electrolyte and mixed-acid electrolyte.

	Heat capacity $[JmL^{-1}K^{-1}]$	**Thermal coefficient** $[mVK^{-1}]$	**Equilibrium voltage**	**Thermoneutral voltage**
CE	4.2	-1.16	1.38	1.72
MAE	3.9	-0.80	1.44	1.67

Using the value of heat dissipated while the battery charges, the result yields $0.085K$. This difference is considered negligible and thus, no heat exchanger will be considered in the design. The literature considers heat exchangers when the temperature rise during the pass of fluid through the stacks is less than $25°C$.

Pumps

The correct design for pumps is mandatory as it is a main component in the solution, as it has previously been explained. The shaft power of the pumps can be calculated using the following Equations:

$$W = \frac{F_A \times \Delta p}{\varepsilon_i} \tag{4.18}$$

$$\varepsilon_i = (1 - 0.12 F_A^{-0.27})(1 - \mu^{0.8}) \tag{4.19}$$

ε_i is the intrinsic efficiency of the pump and depends on the viscosity of the electrolyte, μ, and the actual flow rate of vanadium ion solution, F_A.

The viscosity of the electrolyte is not easy to estimate, as data is not readily available. Besides,the concentration of sulphide-bisulphide ions is not given in Tokuda's articles [66] nor [65]. However, its effect on the calculation of efficiency is not that relevant. Studies in [49] estimate a viscosity of $8cP = 8mPa \cdot s$ for 2M Vanadium solution. On another note, refer to Figure 4.7 from [76]. [76] carries out an intensive study on the effect of SOC on the electrolyte viscosity. In this paper the value of the viscosity ranges from $1.2mPA \cdot s$ to $1.4mPA \cdot s$.

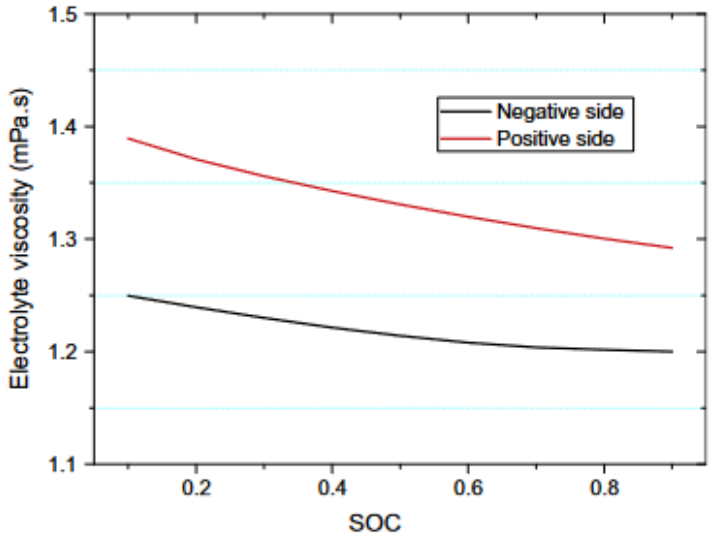

Figure 4.7 Variations in the electrolyte viscosity with SOC in the positive and negative half-cells.

Regardless of these observations, this difference in value only shows a difference of one percentage point on the efficiency. Therefore, a value of $1.3cP$ is taken from [76] as [49] deals with supersaturated vanadium electrolyte.

On another note, a value of of 2 bar for the pressure drop is assumed, that is $2 \cdot 10^5 Pa$.

Lastly, it's relevant to note that in these equations F_A must be in $\frac{m^3}{s}$.

In turn this yields:

$$\varepsilon = 70.5\% \tag{4.20}$$

$$W = 10.6kW \tag{4.21}$$

In order to calculate the costs of this pump, *A guide to chemical engineering design and economics* [68] by Ulrich will be used. Specifically refer to Appendix B.2, where the graphs are attached. In this way, a nickel alloy centrifugal pump and a ratio dollar-euro of $0.94\frac{€}{\$}$ is assumed, giving:

$$Cp = 0.94\frac{€}{\$} \times 7000\$ = 6580€ \tag{4.22}$$

$$F_M = 3.5 \tag{4.23}$$

$$F_p = 1 \tag{4.24}$$

$$F_{BM} = 7 \tag{4.25}$$

Therefore, for one pump:

$$CBM = 46060€ \tag{4.26}$$

Cell stack components

Here, the following costs will be contemplated:

- Ion-exchange membrane

- Current collectors
- Carbon felt electrodes

In order to derive an estimation of these costs, the cost per squared meter is considered for each component. Each 20kW battery system has 60 cells in series, and 24 of these systems are arranged to form the 450 kW battery. So, firstly keeping in mind the 20-kW battery system:

- 60 ion-exchange membranes must be considered (one per cell)
- 61 current collectors must be considered, due to adjacent cells sharing one common current collector
- 120 carbon felt electrodes (two per cell)

Multiplying this by 24, as there are 24 of these system yields the number of elements to be considered, that is:

- 1440 ion-exchange membranes must be considered (one per cell)
- 1464 current collectors must be considered, due to adjacent cells sharing one common current collector
- 2880 carbon felt electrodes (two per cell)

Since [66] explicitly accounts for the area of one electrode to be $5000cm^2$, it will be assumed that the area of one IEM and one current collector is the same due to the way RFBs are designed. On another note, for this type of equipment, $C_{BM} = 1.2 \times C_p$. [68]
In summary, the following data is used:

Table 4.6 Calculation of cost of items in cell stacks.

Element	Cost in €per m^2	Number	m^2 required	Total cost in €(C_p)	Total cost in €(C_{BM})
IEM	282	1440	720	203040	243648
Current collectors	75.2	1464	732	55046.4	66055.7
Carbon felt	47	2880	1440	67680	81216

The costs per squared meter come from [42] and [41].

Additional equipment

This subsection considers the cost of additional equipment also part of the system: Power Conversion System (PCS), power transformer, and breakers, contacts and cabling. The costs are considered per kW and obtained from [41]. These are estimates from the The Electric Power Research Institute (EPRI) projected onto 2025. Carrying out the calculations results in:

Table 4.7 Calculation of PCS and associated items' costs.

Element	**Cost in €per kW**	**Total cost in €(C_p)**	**Total cost in €C_{BM}**
PCS	188	84600	101520
Transformer	33.84	15228	18273.6
Breakers, contacts and cabling	26.45	11903.22	14283.86
Total PCS and associated items	134077.46		

Annualized cost

Starting from Level 3 Analysis, the capital costs are annualized. This includes annual expenses, the cost of capital, and equipment depreciation. The annual expenses are directly proportional to fixed capital as indicated in Table 4.8.

Table 4.8 Annual expenses Proportional to Fixed Capital.

Capital-related cost item	Fractions of fixed capital
Maintenance and repairs	0.06
Operating supplies	0.01
Overhead, etc.	0.03
Taxes and insurance	0.03
General	0.01
Total	0.14

The cost of capital considers the required return on investment for a given capital outlay. The required return on investment will vary among companies, and it is assumed for this case to be 10%. Annualized interest on invested capital expressed as a fraction of the initial capital investment is calculated with Equation 4.27.

$$f_{RI} = \frac{n(\frac{i(1+i)^n}{(1+i)^n-1}) - 1}{n} \tag{4.27}$$

The service life of the components n, is assumed to be 15 years. The annualized cost of components may be calculated by:

$$AC = C_{cost}(0.14 + f_{RI} + f_D) == C_{cost} \times 0.27 \tag{4.28}$$

In summary, these are the results:

Table 4.9 Level 3 Capital Costs.

Item	Total annualized cost
Stacks	106 124 EUR
Pumps	25 008 EUR
PCS and associated items	36 399 EUR
Total	**167 531 EUR**

Unluckily this value is greater than the maximum yearly economic potential reached in Level 2, i.e 167 531 EUR is greater than the previously calculated 130 000 EUR. Therefore, already in Level 3 this battery system is unfeasible. Refer to Figure 4.8.

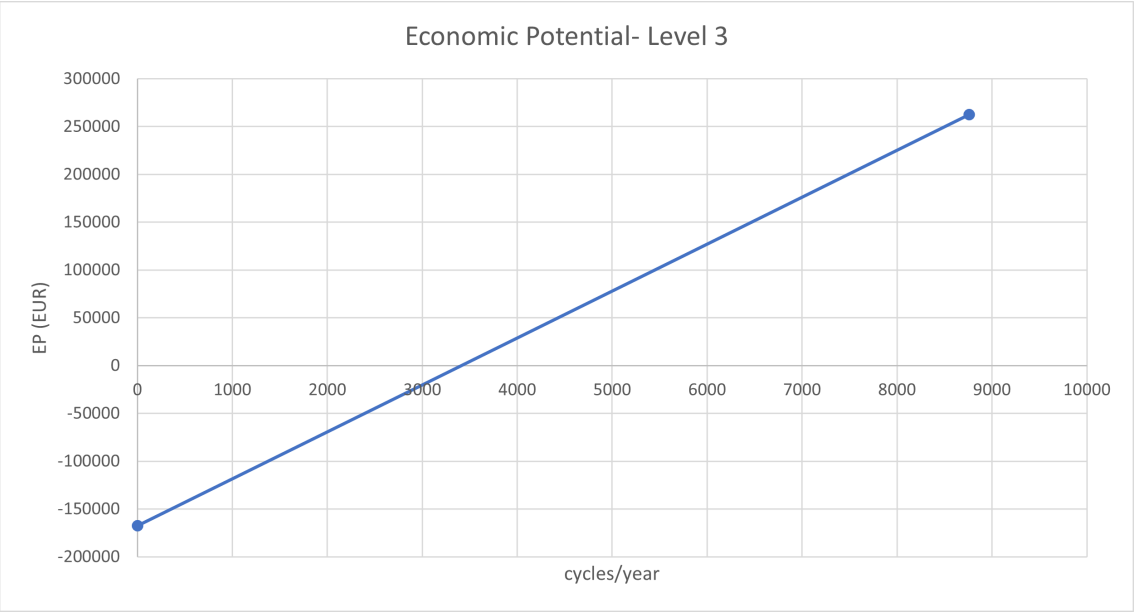

Figure 4.8 Level 3 Economic Potential.

From it, it becomes noticeable that the point when the battery becomes feasible is starting from cycle number 3413.

4.3.5 Level 4 Analysis

Even if the solution is not feasible, the parts of the battery that have not been calculated, that is those related to its capacity will be worked out so that these numbers can be used in a brief comparison carried out in Section 4.4.

The first step is to calculate the volume of solution required. Since it's a VRB, it is known that one mole of ions will produce one mole of electrons when oxidized or reduced. Equation 4.29 applies to calculate the moles of vanadium ions:

$$M_V = \frac{I_S \times \tau_c \times N_c \times N_s}{F} \tag{4.29}$$

, where:

- M_V is the total amount of vanadium needed for the battery in mol
- I_S is the current through a stack in amperes
- τ_c is the time to charge or discharge the battery in seconds
- N_c is the number of cells in a stack
- N_s is the number of stacks in the battery

Nevertheless, it will be assumed that the state of charge ranges rfom 0.20 to 0.80. This means that excess moles of vanadium ions are required. In this way,

$$V_T = \frac{M_V}{M_U - M_L} \tag{4.30}$$

where M_L is the concentration of V(II) at lower charging limit of 0.20, whereas M_U stands for the concentration of V(V) at upper charging limit of 0.80. This yiels a total required volume of 44.7 m^3

for each one of the two tanks.

The volume of electrolyte for the system being considered (Table 4.3) is not given in Tokuda's article. However, Tokuda presents the following table, that allows to check for the veracity of this estimative calculation:

Table 4.10 Various battery system specifications [66].

	20 kW (underground type)	50 kW (high power output type)	50 kW (office building type)
DC output	20 kW		
Battery capacity	160 kWh (20kW x 8 hours)	400 kWh (50 kW x 8 hours)	175 kWh (50 kW x 3.5 hours)
DC voltage (av.)	80 V	115 V	115 V
DC current (av.)	250 A	435 A	435 A
Cell stack	60 cells (series)	90 cells (series)	90 cells (series)
Electrolyte	Vanadium 2 moles/liter Sulfuric acid solution		
Electrolyte tank	Underground rubber tank (4 m^3 x 2)	Underground rubber tank (10 m^3 x 2)	Underground rubber tank (5 m^3 x 2)

Examining the second column of Table 4.10- referring to the 50 kW (high power output type) system, underground rubber tanks of 10 m^3 are used to store electrolyte of a battery system that has approximately half the capacity of our proposed system (400 kWh vs. 900 kWh). Additionally the molarity of the solution is double the one being considered for this system (2M vs. 1M). In other words, the system being studied would be expected to have roughly four times the capacity of this 50 kW high power output type system, that is around 40 m^3. This requirement is completely fulfilled as the calculated volume is 44.7 m^3.

In the first place, the cost of the electrolyte will be estimated. Then, likewise with the tanks themselves.

A price of 6.4 USD per pound (lb) is considered (Refer to Figure 4.9 , which shows the current price of vanadium pentoxide), that is 1.3935 euros per liter of vanadium.

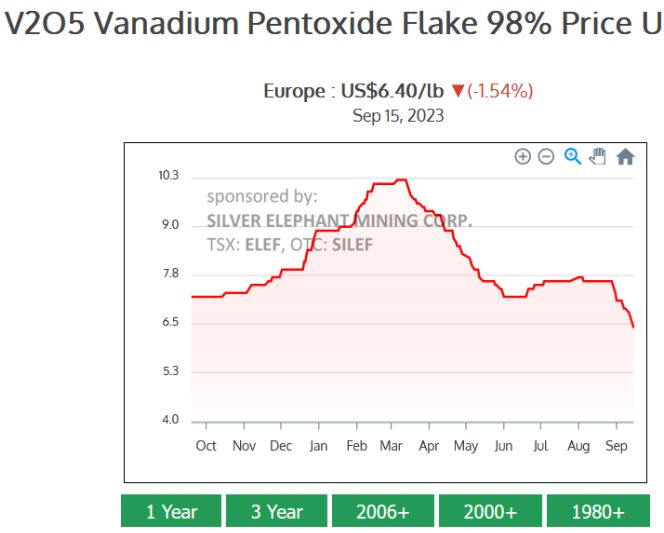

Figure 4.9 Current price of vanadium pentoxide V2O5 [69].

However, it is known that vanadium price fluctuates a lot. For instance within one year, vanadium pentoxide has reached a maximum price of 10.2 dollars per pound and a minimum of 6.4 dollars per pound. Examining the price tendency in three years (Figure 4.10),

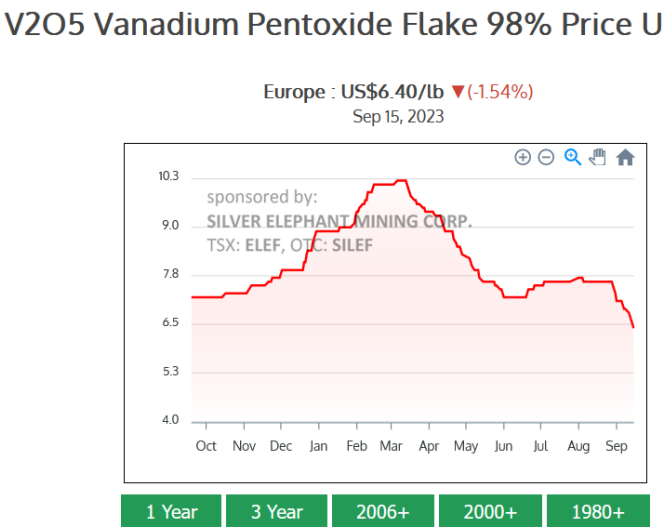

Figure 4.10 Three-years price of vanadium pentoxide V2O5 [69].

it is noticeable that it follows no clear trend- increasing and decreasing continously over time. Therefore, the maximum cost this year of 10.2 dollars per pound is picked for the study. This yields a cost of 2.15 euros per liter. Since a volume of $44774L$ must be considered for each tank- the total calculated cost is 192849.02 €.

In order to be able to establish a comparison, the cost will be annualized analogously as it has been done for the other components. Henceforth, the total annualized cost (AC) of electrolyte:

$$AC_{V_2O_5} = 52353.45€ \tag{4.31}$$

Note that the required sulphuric acid and water is considered negligible in terms of cost.

On the other hand, the cost of the tanks must be calculated. In order to do so, Ulrich graphs will be used as per Appendix B.3. Rubber-lined bullets are assumed as it is the closest material to the one specified in the article. This yields:

$$C_{tank} = 10700 \times 0.93 \frac{€}{\$} = 9951\text{euro} \tag{4.32}$$

$$F_{BM} = 2.7 \tag{4.33}$$

$$AC_{tanks} = 14587.75€ \tag{4.34}$$

4.3.6 Level 5 and 6 Analysis

These two analysis will not be executed due to the conclusion of infeasibility that was reached at Level 3. Level 5 deals with the Balance of Plant, including, for instance:

- Costs for construction
- Costs for the control system
- Building ad site preparation costs

Level 6 is named Capital Investment Estimate, and gathers the information from previous steps to create a capital investment table.

4.4 Comparison of capital cost of components

Level 1 to level 4 analysis gives the following annualized costs of components:

Table 4.11 Annualized estimated costs.

Item	Total annualized cost
Stacks	106 124 EUR
Pumps	25 008 EUR
PCS and associated items	36 399 EUR
Tanks	14 587 EUR
V2O5 electrolyte	52 353 EUR
Total	**234 472 EUR**

Put differently, Figure 4.11 represents how cost is distributed among the different components of the 450kW-900kWh battery system.

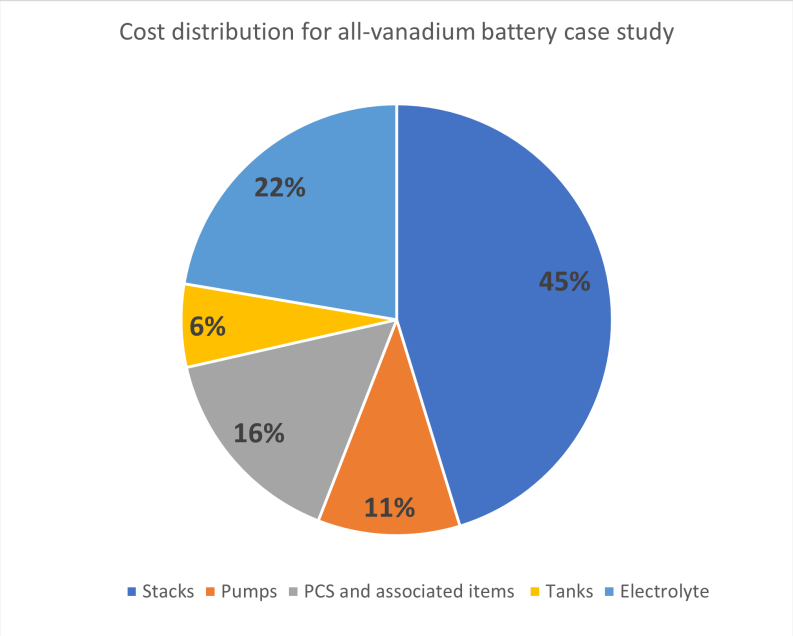

Figure 4.11 Cost distribution for all-vanadium battery case study.

This cost distribution is compared against Viswanathan's analysis in [71]. Refer to Figure 4.12.

As shown below, the distributed cost of electrolyte ranges from 8% for a fourth of an hour battery duration to 43% for four hours battery duration. In the study that has been carried out, the battery duration is 2 hours and the percentage attributed cost is 22%, falling in the range. Similarly, the tanks cost is in both analysis the lowest percentage cost of the entire system.

Thus, it can be concluded that the stacks and the battery electrolyte account for most of the cost in both cases. PCS, tanks and pumps do add in to the overall cost, but do not constitute a great amount of money in the inversion. The percentage attributed to vanadium pentoxide is proportional to the battery duration. Additionally, it is also worth noting that the cell stack constitutes in Viswanathan's analysis [71] a percentage of 60% and 73% of it is due to the separator in the 0.25 MWh battery system. Likewise, for the 4 MWh system 38% of the cost belongs to the cell stack and 71% of it to the separator. In the study case presented throughout the analysis, the numbers remain similar with

45% being attributed to the cell stack, and 62.3% of it is due to the IEM. These conclusions draw out relevant findings on the cost distribution of components among all-vanadium RFBs as they put light on the same discoveries across different system.

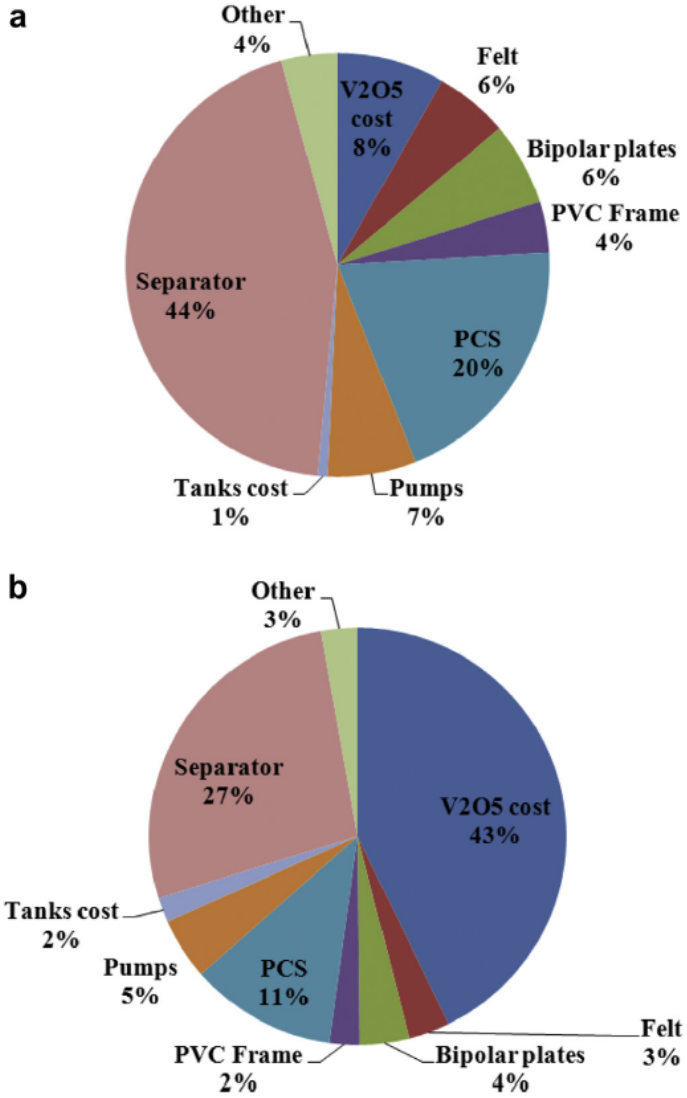

Fig. 6. Distribution of costs for all vanadium Gen 2 for a 1 MW system – a) 0.25 MWh, b) 4 MWh.

Figure 4.12 Distribution of costs for all vanadium Gen 2 for 1 MW system- a) 0.25 MWh, b)4 MWh [71].

A similar cost distribution is also presented by Zhang [78] in Figure 4.13 in terms of the percentage attributed to the capital cost of each component.

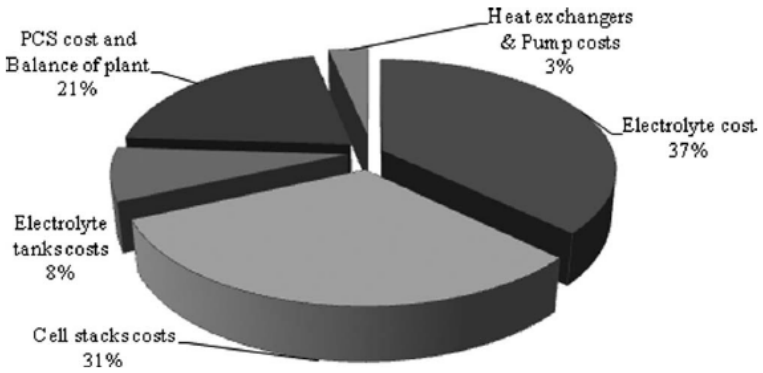

Figure 4.13 Capital cost of the base case VRB [78].

5 Conclusion

This work puts forward the issues and challenges in the development and investigation of Redox Flow Batteries. This pioneering technology opens a way to deal with problems that require a battery system to be solved, such as load leveling or frequency stabilization. Above all, it appears as promising as renewable energy sources must enter the market to counteract the effects of burning fossil fuels as energy source (the latter are a cause of pollution and ceaselessly used cause irreversible climate change effects). Continuity of supply is never guaranteed using renewable resources of energy though. In this way, batteries provide a mean of storing energy and employing it when a renewable energy source is not producing it (e.g. at night in case of PV panels).

As it was already discussed, many battery models exist to compete against redox flow batteries. In general terms, these battery types consist of more mature technology and have a higher energy density, making them more desirable for a vast range of applications.

Efforts have been made to improve Redox Flow Batteries' performance. Most interesting research lines have been drawn towards improving energy efficiency (both coulombic efficiency and voltage efficiency), yet few research lines investigate on the stability of a battery system. Even if improved efficiency result may seem more appealing from a research point of view, the latter point is crucial to make the systems commercially and industrially viable. However, a considerable amount of time is required to prove long-term stability of a system.

Most research lines then focus on improving one of the crucial parts that conform a redox flow battery to prove improved efficiency. This is the case of functional groups being added to electrodes, or the grand amount of treatments that diverse membrane types have been subjected to. Multiple configurations exist and most of them are alive research topics. However, all-vanadium batteries seem to be the most commercially available technology, with big industrial systems being installed. This is due to no cross-mixing contamination being possible, as both electrolytes contain the same species. There is still big room for improving the energy density of these systems as well as the costs associated to it.

While the achievements in membrane and electrolyte research are indeed remarkable, it is important to acknowledge that several significant challenges remain. The integration of these developments into practical RFB systems requires careful consideration of system design, engineering, and optimization. Moreover, safety aspects and environmental impact assessments will need to be addressed rigorously to ensure the technology's viability and acceptance on a large scale.

In order to check viability when considering a real-life application, an analysis was carried out on a technically feasible and stable system already installed in Japan. The results on this analysis prove that they are not economically feasible. In countries like the United States, there is a higher difference between the electricity cost at peak and off-peak hours (one being around ten times greater than the other, as oppossed to Spain, where it is only double). Therefore, installing a redox flow battery system in this network may result in a positive result for feasibility. On the other hand, the percentage distribution of capital costs shows that the membrane and electrolyte solutions are the most expensive items of an all-vanadium system. Definitely, more or less percentage cost is attributed to the electrolyte volume depending on the battery duration. When comparing the estimated cost distribution of the case study with other studies carried out by other authors, the outcomes are therefore consistent and coherent with the existing trends.

Appendix A
Tariff 6.1 TD

endesa

Tarifa Óptima 6.1TD

Muchas gracias por interesarte en nuestras ofertas. Contratando la **Tarifa Óptima** disfrutarás de un precio ajustado y estable para que ahorres y no tengas que preocuparte de las oscilaciones del precio de la energía.

7%

Descuento indefinido sobre el término de energía.

Precios
Precios con descuentos incluidos

Término de Potencia

P1:	P2:	P3:	P4:	P5:	P6:	
23,365215	20,241178	10,727582	8,960662	2,308583	1,548958	€/kW y año
1,947101	1,686765	0,893965	0,746722	0,192382	0,129080	€/kW y mes

Término de Energía (€/kWh)

P1	P2	P3	P4	P5	P6
0,195622	0,175803	0,152045	0,141073	0,116955	0,130619

La potencia a facturar se calculará según corresponda a su tarifa de acceso y potencia contratada, aplicando la facturación por maxímetro o por curva de carga cuarto horaria. La energía será calculada mediante curva de carga horaria.

Las variaciones que se den en los componentes regulados que le son de aplicación, así como nuevos que puedan aparecer, se trasladarán al cliente, tanto al alza como a la baja, sobre el precio base. También se trasladará al cliente cualquier otro cargo que pudiera hacer la distribuidora como energía reactiva, alquiler de equipos de medida, derechos, etc.

Asimismo, los términos de potencia y energía no se actualizan con el valor del IPC.

Precio base del Término de Potencia sin descuento			
	€/kW y año	€/kW y mes	€/kW y dia
P1	23,365215	1,947101	0,064014
P2	20,241178	1,686765	0,055455
P3	10,727582	0,893965	0,029391
P4	8,960662	0,746722	0,024550
P5	2,308583	0,192382	0,006325
P6	1,548958	0,129080	0,004244

El precio base del Término de Energía sin descuento (€/kWh)					
P1	P2	P3	P4	P5	P6
0,210346	0,189036	0,163489	0,151691	0,125758	0,140450

Horario: Los periodos horarios corresponderán en todo momento con los de su tarifa de acceso, mes y ubicación geográfica. Para mayor detalle puede consultar los calendarios en el siguiente enlace, dependiendo de si el suministro está ubicado en Península, Canarias o Baleares: https://www.endesa.com/es/comunicacion/cartera/cliente-empresa

Con permanencia durante 1 año: En caso de resolución unilateral del contrato por parte del Cliente antes de iniciada la primera prórroga, podrá ser aplicada una penalización. Para los suministros con tarifas de acceso 6.1TD, esta cantidad será la equivalente al 10% del precio del Término de Energía del contrato o del precio del Periodo 1 en caso de existir varios periodos, multiplicado por la energía pendiente de suministro (esta energía pendiente de suministro será calculada como el producto del número de días pendientes del Contrato desde la fecha de baja del suministro por la máxima potencia contratada y por un factor 7,1). Esta energía se facturará al precio de la energía, sin descuentos, que tenga el contrato en el momento de la resolución del mismo.

En caso de suministro en alta tensión medido en baja tensión, se aplicarán los mismos recargos por pérdidas que aplique la distribuidora. El exceso de reactiva se facturará al cliente del mismo modo y con el mismo precio que para su tarifa de acceso.

Precio sin impuestos: Impuesto de electricidad (luz - 0,5%) y al importe resultante de lo anterior se aplican los impuestos indirectos: IVA (21%) en Península y Baleares, IGIC en Canarias (0% consumo viviendas con potencia menor o igual a 10kw, resto 3%) e IPSI en Ceuta y Melilla (1%). Tras la publicación del RDL 11/2022 y del RDL 20/2022, temporalmente y si se dieran las circunstancias indicadas en la normativa, se le aplicaría un IVA del 5%.

Tarifa de acceso: **6.1TD hasta 450kW**. Oferta válida para contrataciones **desde el 07/09/2023 hasta el 15/09/2023**.

Figure A.1 Tariff 6.1 TD by Endesa [4].

Appendix B
Graphs for cost estimation by Ulrich

B.1 Heat exchangers

Figure 5-36 Purchased equipment costs for shell and tube and double-pipe heat exchangers. Bare module factors F_{BM}° are derived from Figure 5-38 using material factors given here and pressure factor F_P from Figure 5-37.

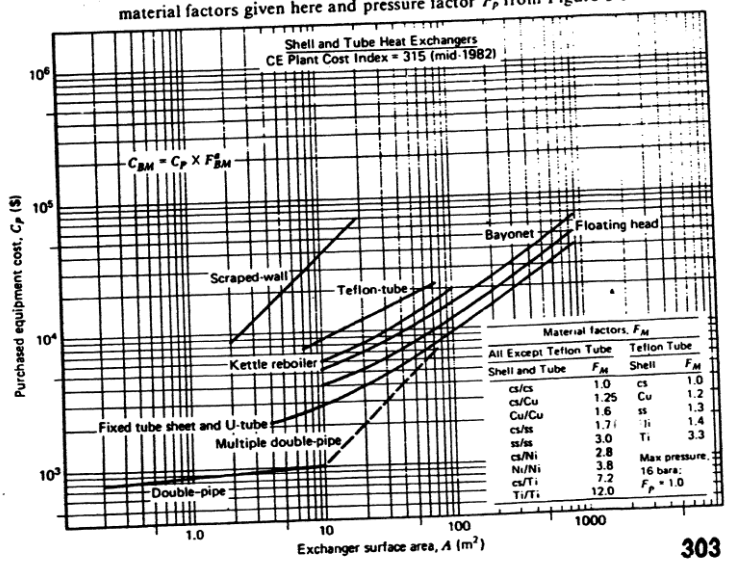

Figure B.1 Purchased equipment cost for heat exchangers [68].

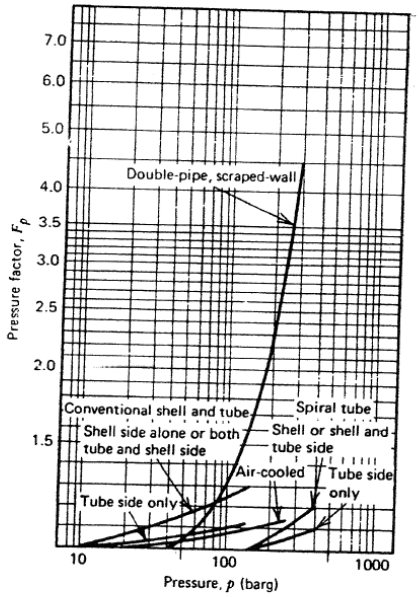

Figure 5-37 Pressure factors (ratio of purchase price of a high pressure heat exchanger to one designed for conventional pressures).

Figure B.2 Pressure factors for high pressure heat exchangers [68].

Figure 5-38 Bare module factors as a function of materials and pressure factors for various classes of heat exchanger.

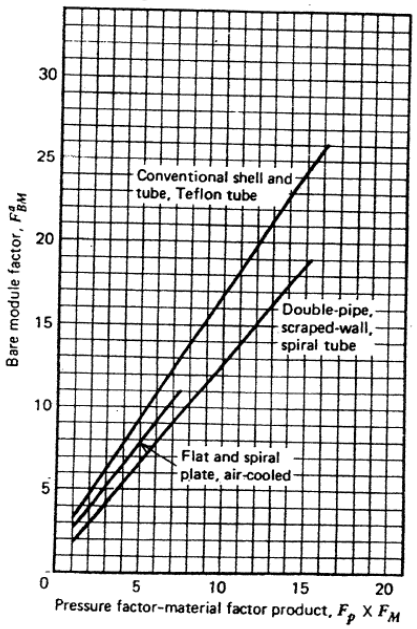

Figure B.3 Bare module factors for heat exchangers [68].

B.2 Pumps

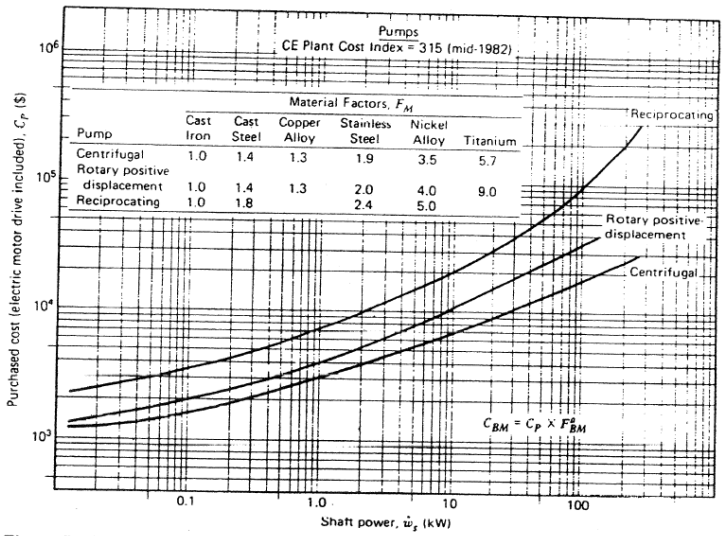

Figure 5-49 Purchased equipment costs for pumps. Shaft power $\dot{w}_S = \dot{q}\Delta p/\epsilon_t$. For unusual service and low capacities, use efficiencies near the lower extremes of ranges given in Table 4-20. Within the sensitivity allowed by a predesign cost estimate, this will compensate for higher priced pumps employed in severe service. Prices are complete with electric motor drives. To substitute other drives, use data in Figures 5-20 and 5-21. For values of F_{BM}^o, see Figure 5-51.

Figure B.4 Purchased equipment cost for pumps [68].

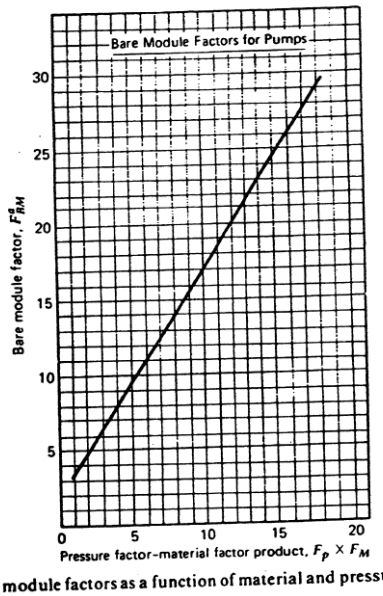

Figure 5-51 Bare module factors as a function of material and pressure factors for pumps.

Figure B.5 Bare module factors for pumps [68].

B.3 Tanks

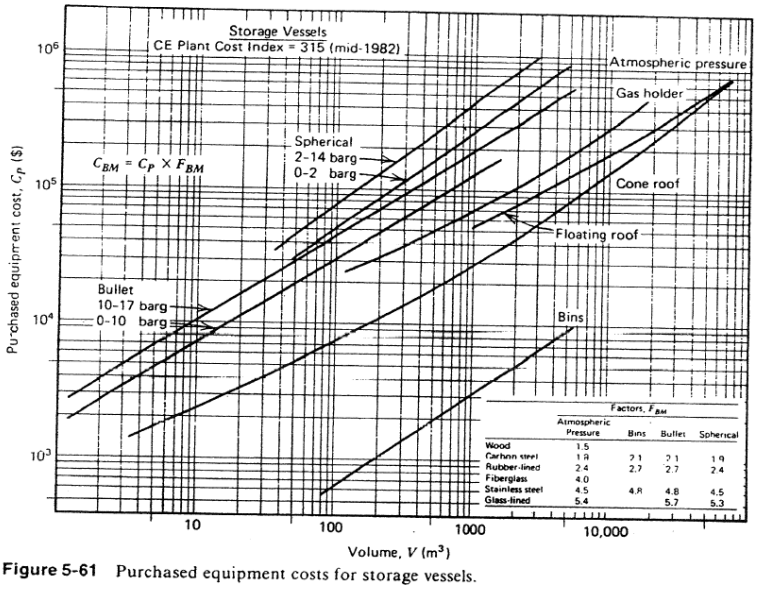

Figure 5-61 Purchased equipment costs for storage vessels.

Figure B.6 Purchased equipment costs for storage vessels [68].

List of Figures

List of Tables

Bibliography

[1] *Materials of construction*, https://www.forbesgroup.co.uk/materials-of-construction/, Jun 2018, The Forbes Group.

[2] *Boe-a-2020-1066*, https://www.boe.es/eli/es/cir/2020/01/15/3/dof/spa/pdf, Jan 2020, Comisión Nacional de los mercados y la competencia - boe.es.

[3] *Pvpc ¿qué es la tarifa regulada?*, https://www.endesa.com/es/blog/blog-de-endesa/luz/pvpc-tarifa-regulada, Jun 2022, Endesa.

[4] *Tarifa Óptima 6.1 td*, https://www.endesa.com/content/dam/endesa-com/endesaclientes/empresas/documentos/es/productos-luz/tarifa-optima/terminos-tarifa-optima.pdf, 2023, Endesa.

[5] Ashley Androsov, *nbsp; bromine-polysulfide redox-flow battery design: Cost analysis*, Ph.D. thesis, Chancellor's Honors Program Projects, 2014.

[6] Itziar Azpitarte, Unai Eletxigerra, Angela Barros, Estibaliz Aranzabe, and Rosalía Cid, *Electrochemical evaluation of different graphite felt electrode treatments in full vanadium redox flow batteries*, Batteries **9** (2023), no. 1.

[7] Emiliano Bellini, *Vanadium redox flow battery to control extreme power ramps in rooftop pv*, PV Magazine (2022).

[8] Christian Blanc and Alfred Rufer, *Understanding the vanadium redox flow batteries*, Paths to Sustainable Energy **18** (2010), no. 2, 334–336.

[9] William A. Braff, Martin Z. Bazant, and Cullen R. Buie, *Membrane-less hydrogen bromine flow battery*, Nature Communications **4** (2013), no. 1, 2346.

[10] Liuyue Cao, Maria Skyllas-Kazacos, and Dawei Wang, *Electrode modification and electrocatalysis for redox flow battery (rfb) applications*, **4** (2015).

[11] Chih-Hsun Chang, Han-Wen Chou, Ning-Yih Hsu, and Yong-Song Chen, *Development of integrally molded bipolar plates for all-vanadium redox flow batteries*, Energies **9** (2016), 350.

[12] Dongyang Chen, Shuanjin Wang, Min Xiao, and Yuezhong Meng, *Synthesis and characterization of novel sulfonated poly(arylene thioether) ionomers for vanadium redox flow battery applications*, Energy Environ. Sci. **3** (2010), 622–628.

[13] S.C. Chieng, M. Kazacos, and M. Skyllas-Kazacos, *Modification of daramic, microporous separator, for redox flow battery applications*, Journal of Membrane Science **75** (1992), no. 1, 81–91.

[14] J. M. Douglas, *A hierarchical decision procedure for process synthesis*, AIChE Journal **31** (1985), no. 3, 353–362.

[15] Alek Eccles, *Sulfuric acid storage tanks amp; specifications*, *https://www.protank.com/sulfuric-acid*, Feb 2019, Protank.

[16] S Eckroad, *Vanadium redox flow batteries: An in-depth analysis*, EPRI, 2007.

[17] R. F. Gahn, N. H. Hagedorn, and J. S. Ling, *Single cell performance studies on the FE/CR Redox Energy Storage System using mixed reactant solutions at elevated temperature*, IECEC '83; Proceedings of the Eighteenth Intersociety Energy Conversion Engineering Conference, Volume 1, vol. 4, January 1983, pp. 1647–1652.

[18] Enrique García-Quismondo, Ignacio Almonacid, Maria Ángeles Cabañero Martínez, Veselin Miroslavov, Enrique Serrano, Jesús Palma, and Juan Pedro Alonso Salmerón, *Operational experience of 5 kw/5 kwh all-vanadium flow batteries in photovoltaic grid applications*, Batteries **5** (2019), no. 3.

[19] Por Gestoriaenergetica and Gestoriaenergetica, *La luz sube mas de un 80en la última década*, Aug 2016.

[20] Katharine V. Greco, Antoni Forner-Cuenca, Adrian Mularczyk, Jens Eller, and Fikile R. Brushett, *Elucidating the nuanced effects of thermal pretreatment on carbon paper electrodes for vanadium redox flow batteries*, ACS Applied Materials & Interfaces **10** (2018), no. 51, 44430–44442, PMID: 30335358.

[21] Zhangxing He, Yanrong Lv, Tianao Zhang, Ye Zhu, Lei Dai, Shuo Yao, Wenjie Zhu, and Ling Wang, *Electrode materials for vanadium redox flow batteries: Intrinsic treatment and introducing catalyst*, Chemical Engineering Journal **427** (2022), 131680.

[22] John W. Hill, Terry Wade McCreary, and Doris K. Kolb, *Chemistry for changing times*, Pearson, 2021.

[23] Aaron Hollas, Xiaoliang Wei, Vijayakumar Murugesan, Zimin Nie, Bin Li, David Reed, Jun Liu, Vincent Sprenkle, and Wei Wang, *A biomimetic high-capacity phenazine-based anolyte for aqueous organic redox flow batteries*, Nature Energy **3** (2018), no. 6, 508–514.

[24] Brian Huskinson, Michael P. Marshak, Michael R. Gerhardt, and Michael J. Aziz, *Cycling of a quinone-bromide flow battery for large-scale electrochemical energy storage*, ECS Transactions **61** (2014), no. 37, 27.

[25] Brian Huskinson, Michael P. Marshak, Changwon Suh, Süleyman Er, Michael R. Gerhardt, Cooper J. Galvin, Xudong Chen, Alán Aspuru-Guzik, Roy G. Gordon, and Michael J. Aziz, *A metal-free organic–inorganic aqueous flow battery*, Nature **505** (2014), no. 7482, 195–198.

[26] Gab-Jin Hwang and H. Ohya, *Preparation of cation exchange membrane as a separator for the all-vanadium redox flow battery*, Journal of Membrane Science **120** (1996), no. 1, 55–67.

[27] Xi Gao Jian, Chun Yan, Hua Min Zhang, Shou Hai Zhang, Cheng Liu, and Ping Zhao, *Synthesis and characterization of quaternized poly(phthalazinone ether sulfone ketone) for anion-exchange membrane*, Chinese Chemical Letters **18** (2007), no. 10, 1269–1272.

[28] Chr Klixbull Jorgensen, *Inorganic complexes*, Academic Press, 1963.

[29] Gareth Kear, Akeel A. Shah, and Frank C. Walsh, *Development of the all-vanadium redox flow battery for energy storage: a review of technological, financial and policy aspects*, International Journal of Energy Research **36** (2012), no. 11, 1105–1120.

[30] Ki Jae Kim, Min-Sik Park, Young-Jun Kim, Jung Ho Kim, Shi Xue Dou, and M. Skyllas-Kazacos, *A technology review of electrodes and reaction mechanisms in vanadium redox flow batteries*, J. Mater. Chem. A **3** (2015), 16913–16933.

[31] Soowhan Kim, Timothy B. Tighe, Birgit Schwenzer, Jingling Yan, Jianlu Zhang, Jun Liu, Zhenguo Yang, and Michael A. Hickner, *Chemical and mechanical degradation of sulfonated poly(sulfone) membranes in vanadium redox flow batteries*, Journal of Applied Electrochemistry **41** (2011), no. 10, 1201–1213 (English (US)), Funding Information: Pacific Northwest National Laboratory (PNNL) is a multiprogram laboratory operated by Battelle Memorial Institute for the Department of Energy under Contract DE-AC05-76RL01830. Funding Information: Acknowledgments The work is supported by the Office of Electricity (OE Delivery Energy Reliability (OE), U.S. Department of Energy (DOE) under contract DE-AC05-76RL01830. Solvay Advanced Polymers is acknowledged for the donation of Radel polymer. The authors thank Dr. Daiwon Choi and Dr. Tak Keun Oh for SEM/EDS analyses.

[32] Min Eui Lee, Hyoung-Joon Jin, and Young Soo Yun, *Synergistic catalytic effects of oxygen and nitrogen functional groups on active carbon electrodes for all-vanadium redox flow batteries*, RSC Adv. **7** (2017), 43227–43232.

[33] Wenyue Li, Jianguo Liu, and Chuanwei Yan, *Graphite–graphite oxide composite electrode for vanadium redox flow battery*, Electrochimica Acta **56** (2011), no. 14, 5290–5294.

[34] T.M. Lim, M. Ulaganathan, and Q. Yan, *Chapter 14 - advances in membrane and stack design of redox flow batteries (rfbs) for medium- and large-scale energy storage*, Advances in Batteries for Medium and Large-Scale Energy Storage (Chris Menictas, Maria Skyllas-Kazacos, and Tuti Mariana Lim, eds.), Woodhead Publishing Series in Energy, Woodhead Publishing, 2015, pp. 477–507.

[35] Imperial College London, *What are redox flow batteries and why are they important?*, *https://www.youtube.com/watch?v=t9zwgL7UpDA*, Nov 2021, YouTube.

[36] Kyle Lourenssen, James Williams, Faraz Ahmadpour, Ryan Clemmer, and Syeda Tasnim, *Vanadium redox flow batteries: A comprehensive review*, Journal of Energy Storage **25** (2019), 100844.

[37] Qingtao Luo, Huamin Zhang, Jian Chen, Dongjiang You, Chenxi Sun, and Yu Zhang, *Preparation and characterization of nafion/speek layered composite membrane and its application in vanadium redox flow battery*, Journal of Membrane Science **325** (2008), no. 2, 553–558.

[38] Zhensheng Mai, Huamin Zhang, Xianfeng Li, Cheng Bi, and Hua Dai, *Sulfonated poly(tetramethydiphenyl ether ether ketone) membranes for vanadium redox flow battery application*, Journal of Power Sources **196** (2011), no. 1, 482–487.

[39] T. Mohammadi and M.Skyllas Kazacos, *Modification of anion-exchange membranes for vanadium redox flow battery applications*, Journal of Power Sources **63** (1996), no. 2, 179–186.

[40] T. MOHAMMADI and M.SKYLLAS KAZACOS, *Evaluation of the chemical stability of some membranes in vanadium solution*, Journal of Applied Electrochemistry **27** (1997), no. 2, 153–160.

[41] Kendall Mongird, Vilayanur V. Viswanathan, Patrick J. Balducci, Md Jan E. Alam, Vanshika Fotedar, V S. Koritarov, and Boualem Hadjerioua, *Energy storage technology and cost characterization report*, (2019).

[42] Mark Moore, Robert Counce, Jack Watson, T.A. Zawodzinski, and H. Kamath, *A step-by-step design methodology for a base case vanadium redox-flow battery*, **46** (2012), 239–250.

[43] Mark Alan Moore, *nbsp; a base case design and capital cost analysis of an all vanadium redox-flow battery*, Ph.D. thesis, Chancellor's Honors Program Projects, 2013.

[44] Elizabeth Hope Mouron, *nbsp; the economic potential of the all-vanadium redox flow battery with a focus on state of charge*, Ph.D. thesis, Chancellor's Honors Program Projects, 2011.

[45] OCU, *El precio de la luz en septiembre*, *https://www.ocu.org/vivienda-y-energia/gas-luz/informe/precio-luz*, Jun 2023.

[46] V.M. Ortiz-Martínez, L. Gómez-Coma, G. Pérez, A. Ortiz, and I. Ortiz, *The roles of ionic liquids as new electrolytes in redox flow batteries*, Separation and Purification Technology **252** (2020), 117436.

[47] Feng Pan and Qing Wang, *Redox species of redox flow batteries: A review*, Molecules **20** (2015), no. 11, 20499–20517.

[48] Sonal Patel, *Grid-scale iron-chromium redox flow battery connected*, POWER (2014).

[49] Faizur Rahman, *Optimization of supersaturated vanadium electrolyte for high energy density vanadium redox battery*, 10 2000.

[50] Danick Reynard, C.R. Dennison, Alberto Battistel, and Hubert H. Girault, *Efficiency improvement of an all-vanadium redox flow battery by harvesting low-grade heat*, Journal of Power Sources **390** (2018), 30–37.

[51] Hannah Ritchie, Pablo Rosado, and Max Roser, *Energy production and consumption*, Our World in Data (2020), https://ourworldindata.org/energy-production-consumption.

[52] David Rivero Bermúdez, *Sistemas de almacenamiento de energía. baterías de flujo*, (2021).

[53] Eduardo Sanchez-Diez, Edgar Ventosa, Massimo Guarnieri, Andrea Trovò, Cristina Flox, Rebeca Marcilla, F. Soavi, Petr Mazúr, Estibaliz Aranzabe, and Raquel Ferret, *Redox flow batteries: Status and perspective towards sustainable stationary energy storage*, Journal of Power Sources **481** (2021), 228804.

[54] Dominik Schulte, J Drillkensb, BSchulteb, and Dirk Uwe Sauer, *Nafion hybrid membranes for use in redox flow batteries*, ECS Transactions **25** (2010), 247–255.

[55] Birgit Schwenzer, Soowhan Kim, M. Vijayakumar, Zhenguo Yang, and Jun Liu, *Correlation of structural differences between nafion/polyaniline and nafion/polypyrrole composite membranes and observed transport properties*, Journal of Membrane Science **372** (2011), no. 1, 11–19.

[56] Birgit Schwenzer, Jianlu Zhang, Soowhan Kim, Liyu Li, William Liu, and Zhenguo Yang, *Membrane development for vanadium redox flow batteries*, ChemSusChem **4** (2011), 1388–406.

[57] Joan I. Senyk, Darrell D. Ebbing, and Larry K. Krannich, *Study guide: General chemistry, ebbing*, Houghton Mifflin, 1996.

[58] Maria Skyllas-Kazacos, George Kazacos, Grace Poon, and Hugh Verseema, *Recent advances with unsw vanadium-based redox flow batteries*, International Journal of Energy Research **34** (2010), no. 2, 182–189.

[59] Kevin Spellman, Kendrick Stiles, and Ian Little, *nbsp; economic report on vanadium redox flow battery with optimization of flow rate*, Ph.D. thesis, Chancellor's Honors Program Projects, 2013.

[60] Theresa Sukkar and Maria Skyllas-Kazacos, *Water transfer behaviour across cation exchange membranes in the vanadium redox battery*, Journal of Membrane Science **222** (2003), no. 1, 235–247.

[61] Theresa Sukkar and Maria Skyllas-Kazacos, *Membrane stability studies for vanadium redox cell applications*, Journal of Applied Electrochemistry **34** (2004), no. 2, 137–145.

[62] B. Sun and M. Skyllas-Kazacos, *Modification of graphite electrode materials for vanadium redox flow battery application—i. thermal treatment*, Electrochimica Acta **37** (1992), no. 7, 1253–1260.

[63] Chenxi Sun, Jian Chen, Huamin Zhang, Xi Han, and Qingtao Luo, *Investigations on transfer of water and vanadium ions across nafion membrane in an operating vanadium redox flow battery*, Journal of Power Sources **195** (2010), no. 3, 890–897.

[64] Michael W Thielke, Gengyu Tian, and Ana Jorge Sobrido, *Sustainable electrodes for the next generation of redox flow batteries*, Journal of Physics: Materials **5** (2022), no. 2, 024004.

[65] N. Tokuda, M. Furuya, Y. Kikuoko, Y. Tsutui, T. Kumamoto, and T. Kanno, *Development of a redox flow (rf) battery for energy storage*, Proceedings of the Power Conversion Conference-Osaka 2002 (Cat. No.02TH8579), vol. 3, 2002, pp. 1144–1149 vol.3.

[66] N. Tokuda, Toru Kanno, T. Hara, T. Shigematsu, Y. Tsutsui, A. Ikeuchi, T. Itou, and T. Kumamoto, *Development of redox flow battery system*, SEI Technical Review **50** (2000), 88–94.

[67] Nobuyuki Tokuda, Takahiro Kumamoto, Toshio Shigematsu, Hiroshige Deguchi, Takefumi Ito, Noriyasu Yoshikawa, and Takushi Hara, *Development of a redox flow battery system*, SUMITOMO ELECTRIC TECHNICAL REVIEW-ENGLISH EDITION- (1998), 88–94.

[68] Gael D. Ulrich, P. T. Vasudevan, and Gael D. Ulrich, *A guide to chemical engineering process design and economics: A practical guide*, CRC, 2003.

[69] VanadiumPrice.com, *https://vanadiumprice.com/*.

[70] M. Vijayakumar, M.S. Bhuvaneswari, P. Nachimuthu, Birgit Schwenzer, Soowhan Kim, Zhenguo Yang, Jun Liu, Gordon L. Graff, S. Thevuthasan, and Jianzhi Hu, *Spectroscopic investigations of the fouling process on nafion membranes in vanadium redox flow batteries*, Journal of Membrane Science **366** (2011), no. 1, 325–334.

[71] Vilayanur Viswanathan, Alasdair Crawford, David Stephenson, Soowhan Kim, Wei Wang, Bin Li, Greg Coffey, Ed Thomsen, Gordon Graff, Patrick Balducci, Michael Kintner-Meyer, and Vincent Sprenkle, *Cost and performance model for redox flow batteries*, Journal of Power Sources **247** (2014), 1040–1051.

[72] Francisco Javier Vázquez Galván, *Redox flow batteries: From vanadium to earth abundant organic molecules (quinones)*, Ph.D. thesis, 2019.

[73] Jingyu Xi, Zenghua Wu, Xinping Qiu, and Liquan Chen, *Nafion/sio2 hybrid membrane for vanadium redox flow battery*, Journal of Power Sources **166** (2007), no. 2, 531–536.

[74] Jingyu Xi, Zenghua Wu, Xiangguo Teng, Yongtao Zhao, Liquan Chen, and Xinping Qiu, *Self-assembled polyelectrolyte multilayer modified nafion membrane with suppressed vanadium ion crossover for vanadium redox flow batteries*, J. Mater. Chem. **18** (2008), 1232–1238.

[75] Dongbo Xing, Shouhai Zhang, Chunxiang Yin, Bengui Zhang, and Xigao Jian, *Effect of amination agent on the properties of quaternized poly(phthalazinone ether sulfone) anion exchange membrane for vanadium redox flow battery application*, Journal of Membrane Science **354** (2010), no. 1, 68–73.

[76] Q. Xu, T.S. Zhao, and C. Zhang, *Effects of soc-dependent electrolyte viscosity on performance of vanadium redox flow batteries*, Applied Energy **130** (2014), 139–147.

[77] Lu Yue, Weishan Li, Fengqiang Sun, Lingzhi Zhao, and Lidan Xing, *Highly hydroxylated carbon fibres as electrode materials of all-vanadium redox flow battery*, Carbon **48** (2010), no. 11, 3079–3090.

[78] Mengqi Zhang, Mark Moore, J. S. Watson, Thomas A. Zawodzinski, and Robert M. Counce, *Capital cost sensitivity analysis of an all-vanadium redox-flow battery*, Journal of The Electrochemical Society **159** (2012), no. 8, A1183.

[79] X.L. Zhou, Y.K. Zeng, X.B. Zhu, L. Wei, and T.S. Zhao, *A high-performance dual-scale porous electrode for vanadium redox flow batteries*, Journal of Power Sources **325** (2016), 329–336.

1. Introducción

La energía es la materia prima que sustenta la vida humana y contribuye al desarrollo de la industrialización y estilo de vida. A medida que la digitalización se impone junto con el desarrollo tecnológico y la electrificación, se registra un mayor consumo de energía a lo largo de los años.

El petróleo y el carbón son las fuentes que reportan mayor consumo de energía primaria. El aumento del consumo de energía en el siglo XIX es bastante insignificante si se compara con el aumento registrado en el siglo XX. El hecho de que el petróleo y el carbón sean las fuentes principales pone de manifiesto varios obstáculos [52]:

- Los precios de los combustibles fósiles están subiendo mucho debido a la escasez de esta fuente y a la complicación que conlleva extraer energía de ellos.
- Los combustibles fósiles contribuyen fuertemente a la contaminación y al cambio climático, debido a la emisión de gases de efecto invernadero que se produce al quemarlos para obtener energía de los mismos
- La demanda de energía es casi exponencialmente creciente

Esto hace que la investigación se centre en encontrar fuentes de energía alternativas. Existen múltiples fuentes de energía renovable que posteriormente pueden almacenarse mediante sistemas de baterías, tales como, pero no limitadas a la energía solar, la energía eólica, la energía hidráulica, la energía del agua de mar, la energía geotérmica y la energía de la biomasa y los residuos.

Muchos sistemas de almacenamiento de energía, entre ellos múltiples tipos de baterías coexisten en el mercado de almacenamiento energético. Entre las baterías, se pueden destacar las de plomo-ácido o las de ión-litio. Sin embargo, lo que diferencia a las baterías de flujo redox de otros tipos de baterías es:

- Su capacidad para aumentar/disminuir físicamente la potencia y la capacidad de forma independiente (son dos magnitudes desacopladas)
- Bajo nivel de autodescarga
- Nivel de degradación prometedoramente bajo debido a los principios químicos a los que obedecen.

Aún queda mucho por investigar sobre este tipo de sistema de baterías para que sea viable y útil en las aplicaciones requeridas, como se verá más adelante. Sin embargo, son las baterías de flujo redox son candidatas a contribuir a la descarbonización del sector eléctrico.

2. Principio de funcionamiento de las Baterías de Flujo Redox

Como sugiere su nombre, las RFB funcionan gracias a las reacciones químicas redox que se producen en ellas. Para empezar, describiremos su principio de funcionamiento con ayuda de la Figura 7.

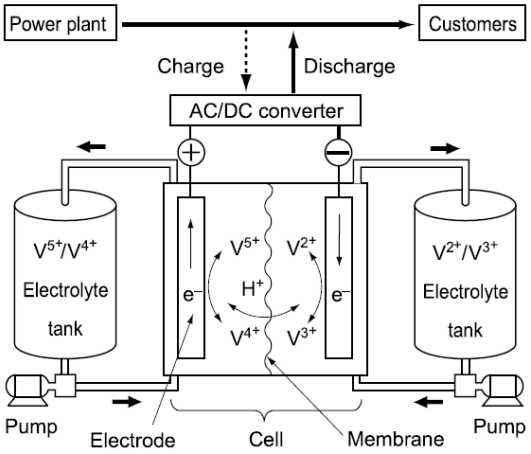

Figure 7 Principio de funcionamiento de RFBs [67].

Aunque el esquema presentado en la Figura 7 muestra un sistema totalmente de vanadio, las partes o componentes son equivalentes independientemente de los compuestos que participen en las reacciones.

Como se aprecia en este esquema los componentes clave que deben estar presentes son:

- **Electrolito positivo** (generalmente también conocido como catolito)
- **Electrolito negativo** (generalmente también conocido como anolito)
- Dos **tanques** para almacenar ambos electrolitos
- Dos **bombas** integradas en un sistema de control de caudal
- **Membrana**
- Dos **electrodos**

A partir de la Figura 7,se puede representar que los electrolitos se bombean a través de una pila donde se puede poner o quitar energía de los fluidos cambiando sus estados de oxidación. Dado que

la carga y la descarga se producen en las pilas, estas últimas están directamente relacionadas con la cantidad de energía que el sistema es capaz de suministrar.

Este punto puede enfatizarse afirmando que el diseño es modular [35].

- Si más energía almacenada se requiere, el tamaño de los depósitos puede aumentarse,
- mientras que si hay un mayor requerimiento de potencia, más pilas puedn añadirse

La Figura 8 muestra una representación visual de un conjunto de celdas. Como puede verse, las células se apilan tanto en serie como en paralelo. Apilarlas en serie aumenta la tensión, mientras que apilarlas en paralelo permite obtener una mayor corriente.

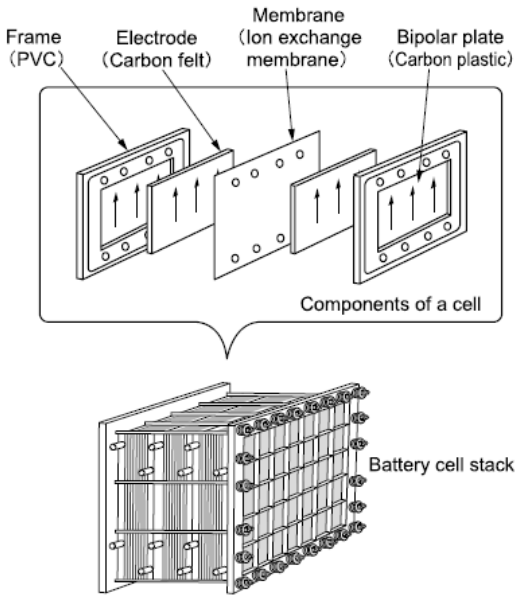

Figure 8 Construcción de un conjunto de celdas [67].

En relación a los **tanques**, contemplarlos más voluminiosos permite almacenar mayor cantidad de electrolito. Las especies activas en este proceso no son otras que los electrolitos. Por tanto, la capacidad de la batería resulta ser directamente proporcional a la cantidad de especies activas que son capaces de someterse a reacciones electroquímicas produciendo energía. Algunos materiales comunes empleados pueden ser [15]:

1. Polietileno de alta densidad (HDPE)
2. Polipropileno (PP)- tanques poly
3. Plástico reforzado con fibra de vidrio (PRFV) - depósitos de fibra de vidrio
4. Acero inoxidable

Los tanques de PRFV son artesanales y costosos de fabricar. Además los tanques de polipropileno tienen alta resistencia a la corrosión, facilitando el mantenimiento. La tendencia del mercado es hacia los tanques de polipropileno.

En cuanto a los **electrodos**, algunos de los materiales más comunes pueden ser, por ejemplo: - Grafito - Fieltro de carbono - Cerámica conductora - Óxidos metálicos mixtos Como se desprende de la lista de ejemplos anterior, los electrodos deben ser materiales altamente conductores, ya que es a través de ellos por donde fluyen los electrones para cargar y descargar la batería. Asimismo,

cuanto mayor sea la superficie de los electrodos, mejor será la reacción electroquímica, ya que proporcionan "los lugares de reacción". Acogen más material activo mejorando la velocidad de transferencia de electrones. Un punto importante a destacar es que los electrodos son "inertes"- no participan en la reacción [10]. Para mejorar la eficiencia de los electrodos, se enumeran diferentes tratamientos investigados: térmico, por ácido, grabado químico, dopaje de heteroátomos, etc. [21]

En cuanto a la membrana, una membrana selectiva de iones ocupa su lugar entre los electrodos positivo y negativo en una pila de flujo Redox. Esta membrana permite que los electrones fluyan a través de ella a la vez que evita la mezcla de los dos electrolitos (anolito y catolito). La membrana selectiva de iones desempeña un papel crucial en el mantenimiento de la separación de cargas y en la prevención de la contaminación cruzada de los electrolitos.

Hay elementos adicionales como los captadores de corriente, sistemas de bombeo y posibles intercambiadores de calor, entre otros.

El principio electroquímico se ejemplifica a continuación mediante las ecuaciones químicas de la batería de vanadio. [11]

$$VO_2{}^+ + 2H^+ + e^- \rightleftharpoons VO^{2+} + H_2O \tag{5.1}$$

$$V^{2+} \rightleftharpoons V^{3+} + e^- \tag{5.2}$$

3. Líneas de investigación y retos

Durante este capítulo se abordan las principales líneas de investigación y hallazgos, que se resumen muy brevemente a continuación.

3.1. Desarrollo de membranas

El estudio se centra en las membranas utilizadas en baterías RFB acuosas.

Se descubren y se somete a pruebas diferentes tipos de membranas:

- Membranas de intercambio de cationes
- Membranas de intercambio de aniones
- Membranas microporosas

La membrana de Nafion es la más popular y se debe principalmente a su capacidad de soportan las condiciones acídicas requeridas.
El principal problema es la falta de testeo en cuanto a la estabilidad a largo plazo. La mayoría de las investigaciones se centran en contribuir a mejorar la eficiencia del sistema.

Diferentes factores se comprueban en las investigaciones, tales como la resistencia específica o la concentración de iones. No obstante, los hallazgos dependen del tipo de membrana. Por ejemplo, en el caso de la membrana S-Radel, tiene lugar mayor degradación de la misma a mayor concentración de iones de vanadio. Se puede ver Figura 9 c) 0.1M de iones de vanadio y d) 1.7M de iones de vanadio.

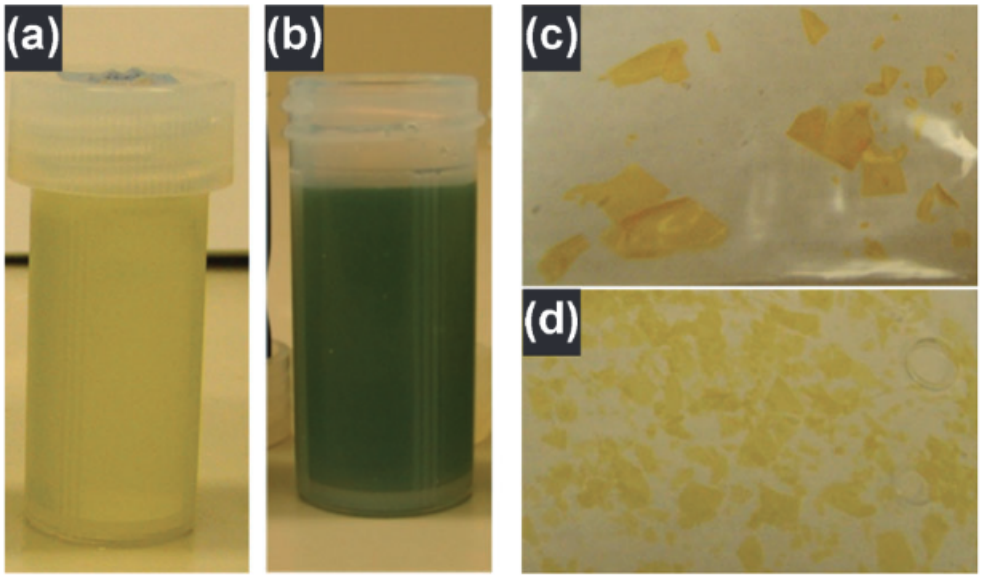

Figure 9 Resultados de degradación de membrana [31].

Otro factor de interés en las membranas es el transporte de agua. Este último es necesario para la conducción ya que contribuye a través del mecanismo de Grotthuss a lo largo del centro de los poros de la membrana. El mecanismo de Grotthuss permite "una transferencia intermolecular de protones entre moléculas de agua en los canales que penetran en la membrana", ya que se trata del "salto" de un ion hidrógeno a través de la permeación a través de la red de moléculas de agua. [36] Por lo tanto, según esta lógica, la conductividad de protones se mejoraría ampliando el tamaño de los poros de las membranas. Sin embargo, esto provocará un mayor grado de contaminación de los electrolitos. Las investigaciones tratarán de encontrar el tamaño óptimo de los poros, ya que al reducirlos se reduce tanto el transporte de iones de vanadio como la conducción a través de la membrana. Otro efecto que tiene que ver con la transferencia de agua es que la transferencia neta de agua hará que el electrolito de una semicelda esté más concentrado y el otro más diluido. Este desequilibrio provocará una disminución de la capacidad y la eficiencia de los VRFB.

Membranas de intercambio de cationes

Un ejemplo es el Nafion. Se descubrió que incluir SiO_2 en la red de canales hidrófilos aumentaba la eficiencia energética, ya que decrementaba el transporte de agua pero con similar conductividad. Observe el proceso en la Figura 10.

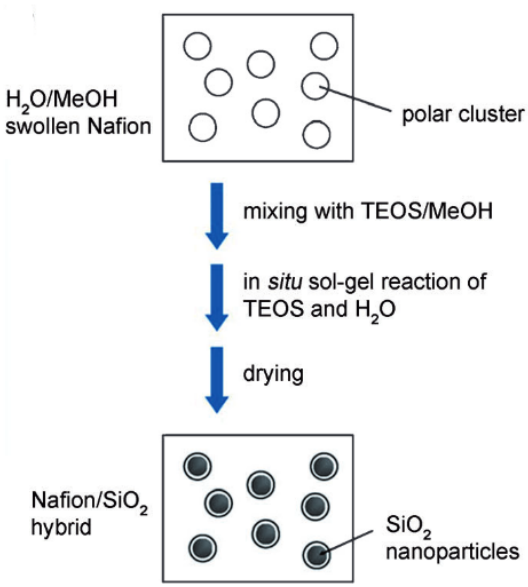

Figure 10 Esquemático de membrana de Nafion modificada con SiO_2 síntesis sol-gel [73].

En otras palabras, se reducía notablemente la permeabilidad de los cationes de vanadio. Ver 11

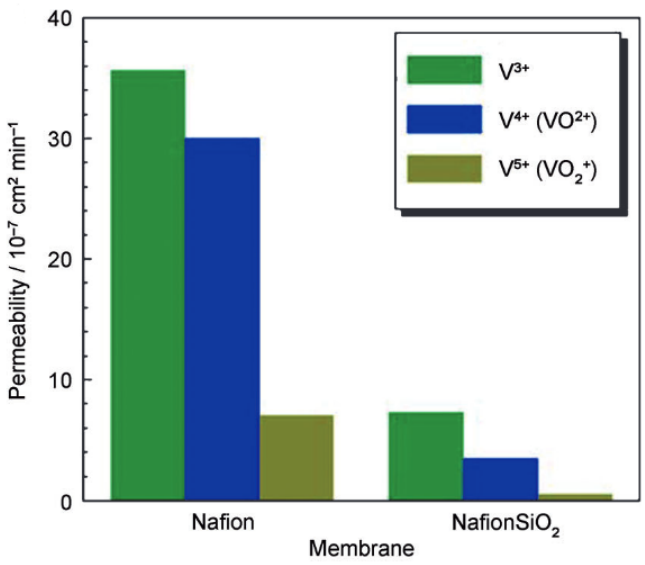

Figure 11 Comparación de permeabilidades de las diferentes especies de iones de Vanadio a través de Nafion Puro y Nafion/SiO_2 [73].

La combinación Nafion/SPEEK también resultó atractiva por tener características de ambos.

Membranas de intercambio de aniones

Uno de los tipos de membrana que quedan por discutir son las membranas de intercambio aniónico. Podrían ser una tecnología prometedora ya que evitarían la mezcla cruzada de todos los cationes de vanadio. De este modo, podrían alcanzarse eficiencias cercanas al 100%. No obstante, al tratarse de una membrana de intercambio aniónico, además de reducir la permeabilidad de los iones de vanadio también dificulta la conducción de protones. Este último efecto sacrifica la eficiencia del

voltaje. [57]

También la estabilidad química y el mayor transporte de agua son cuestiones adicionales. Se están estudiando y esta investigación puede conducir a la construcción de membranas híbridas más eficaces y complejas que permitan mitigar estos problemas.

Otras configuraciones

Existen también algunos estudios sobre las membranas anfotéricas de intercambio iónico. Aunque con resultados prometedores, solo se ha logrado una estabilidad de 50 ciclos hasta el momento.

También se contemplan configuraciones totalmente rompedoras, como eliminar la membrana en celdas HBLFB. Ver Figura 12.

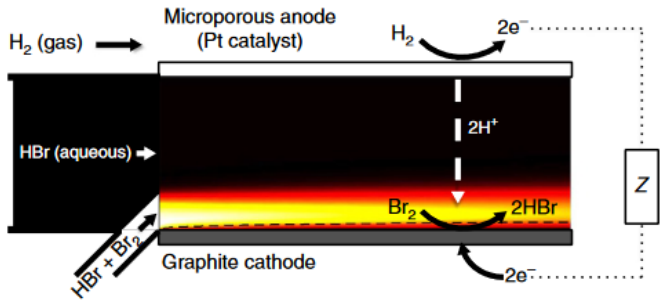

Figure 12 Esquemático del flujo de reactivo dentro de una HBLFB [9].

3.2. Química de los electrolitos y optimización

Se enlistan algunos de los tipos examinados a lo largo del trabajo.

3.2.1. RFB de Vanadio

Propuesto por primera vez por Skyllas-Kazacos, sólo emplea vanadio tanto en el catolito como en el anolito, por lo que la contaminación por cruce no es un obstáculo. Por lo tanto, se puede conseguir una larga vida útil del sistema aprox 5-20 años. [47] La cinética electroquímica rápida con un tiempo de respuesta corto es una ventaja. [53] Como desventajas cabe destacar:

- Fuerte resistencia a la corrosión
- Menor densidad energética que las baterías de iones de litio, por ejemplo

3.2.2. RFB de Hierro-cromio

Esta configuración fue desarrollada principalmente por la NASA [17], proporcionando un voltaje de célula de 1,18V.

Mientras que la reacción catódica muestra una buena reversibilidad y una cinética rápida, la reacción del cromo en el ánodo presenta un cuello de botella: requiere una temperatura de operación elevada y su bajo potencial redox invita a la evolución del H_2. [47]

3.2.3. RFB de Vanadio y oxígeno

Como ventajas:

- Mayor densidad energética
- Se necesita menos cantidad de vanadio, que es caro

Sin embargo, [53]

- La reacción del electrodo positivo muestra un bajo grado de reversibilidad, esto podría solucionarse añadiendo un electrolizador provisto de catalizadores especiales
- Sólo se ha probado a pequeña escala
- La estabilidad a largo plazo es un reto

3.2.4. Baterías de flujo basadas en zinc

Como ventajas, presentan:

- Bajo coste
- Rápida reacción del electrodo
- Alta solubilidad de los iones Zn(II)
- Para el Zn/Ni se exhibe un alto voltaje de celda de 1.73V

Algunas de las desventajas que presentan se mencionan a continuación:

- Menor durabilidad debido a la deposición desigual en el electrodo durante la carga de la batería
- Depósitos dendríticos que conducen al fallo de la célula
- Se produce HER, disminuyendo la eficiencia

4. Caso de estudio: Viabilidad económica

En este capítulo se realizará una aproximación a la viabilidad económica de una Batería de Flujo Redox de Vanadio en España. Para ello, existen dos tareas principales que preceden a este proceso en el siguiente orden:

1. Selección de una metodología de análisis de costes
2. Selección de un modelo de batería viable para aplicar dicho análisis

Dado que la información disponible sobre los distintos sistemas de baterías investigados hasta ahora no es especialmente abundante, existe una estrecha relación entre los pasos mencionados. Se evaluaron diversos ejemplos de análisis de costes. Después de haber examinado algunas de ellas, cabe señalar que no es en absoluto trivial poner en práctica estas metodologías, ya que su complejidad intrínseca las hace depender de datos no fácilmente disponibles ni estimables. No obstante, las observaciones y los resultados obtenidos por ellas se discutirán más adelante como parte de este trabajo. Finalmente la metodología seleccionada se trata de una metodología inspirada en una desarrollada por Douglas, un proceso jerárquico paso a paso utilizado a menudo en las clases de ingeniería química que procede a través de niveles de decisión donde se añaden más detalles al diagrama de flujo en cada paso o nivel del procedimiento de diseño. No obstante, en algunos puntos de la metodología es necesario hacer suposiciones, ya que no se dispone fácilmente de los datos necesarios. [14] [42]

En relación al precio de la electricidad para horas punta y valle se toma como 0.2EUR/kWh y 0.1EUR/kWh respectivamente, de acuerdo con la Tarifa 6.1 TD.

En cuanto al **sistema** [66], el elegido es uno de 450 kW que se instaló en 1996 en la subestación de Tatsumi de Kansai Electric Power Co. Ltd. Es una batería de vanadio y a continuación se presenta su diagrama de bloques:

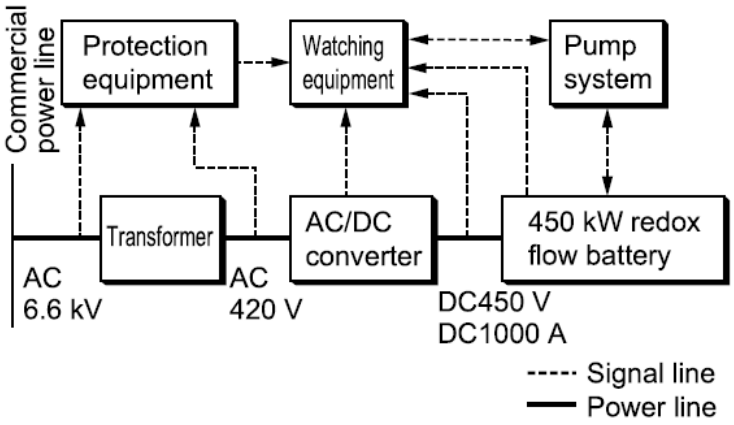

Figure 13 Sistema de 450 kW [66].

Se observa que hay sistemas adicionales que dan soporte a una conexión segura a la red, un transformador y un convertidor CA/CC unidos por una línea de alimentación. Se añaden líneas de señalización para dar cuenta del sistema de bombeo, el equipo de protección y el equipo de vigilancia. El análisis presentado en este apartado estimará los costes de todos los subsistemas unidos por líneas de potencia, así como del sistema de bombeo.

Se presentan y calculan los datos disponibles cuando no se facilitan directamente en el artículo. La batería de 450 kW está formada por pilas de celdas de batería de 18,8 kW cada una, con las siguientes características [66]:

Table 1 Especificación del sistema de 20 kW [66].

Salida DC	18.8 kW
Voltaje DC	75.2 V
Intensidad DC	250 A
Área del electrodo	5000 cm^2
Conjunto de celdas	60 celdas (serie)
Electrolito	Vanadio 1M Solución de ácido sulfúrico

Por tanto, el sistema de baterías se construye apilando pilas de este tipo en serie y en paralelo. En concreto, un módulo se consigue apilando pilas de celdas en una configuración 4P x 2S, lo que significa que un módulo obedece:

$$V_{DC} = 2 \times 75.2V = 150.4V \tag{5.3}$$

$$I_{DC} = 4 \times 250A = 1000A \tag{5.4}$$

Los módulos se apilan en series de tres:

$$V_{DC} = 3 \times 150.4V = 451.2V \approx 450V \tag{5.5}$$

Estos cálculos ejemplifican el hecho de que apilar pilas de células en serie aumenta la tensión, mientras que apilarlas en paralelo aumenta la corriente. Así, las especificaciones fácilmente disponibles de todo el sistema son:

Table 2 Especificación del sistema de 450 kW.

Salida DC	450 kW
Capacidad de la batería	900 kWh (450 kW x 2 horas)
Voltaje DC	450 V (av.)
Intensidad DC	1000 A (av.)
Módulo de celda	1 módulo: Conjunto de celdas 4P x 2S Series de 3 módulos
Electrolito	Vanadio 1M Solución de ácido sulfúrico
AC/DC Convertidor	Control PWM

La densidad de corriente es $50\frac{mA}{cm^2}$ [66].

Por otra parte, como ya se ha mencionado, la estabilidad del sistema es obligatoria. La prueba de ciclo de vida del sistema de baterías de 20 kW presenta los siguientes resultados en la Figura 14:

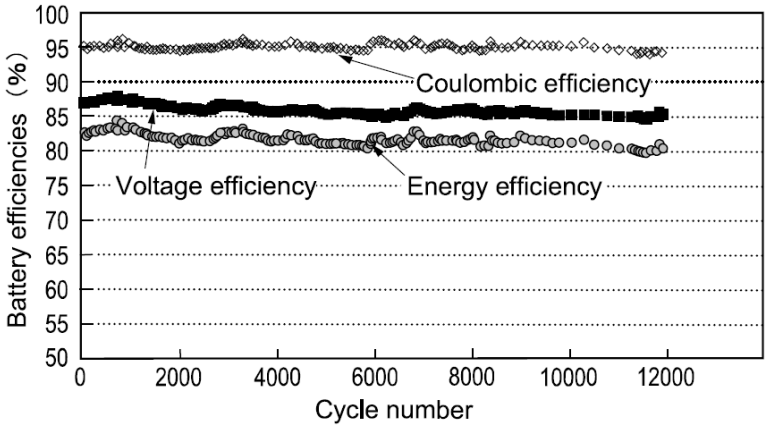

Figure 14 Pruebas de ciclos de vida [66].

A lo largo de 12.000 ciclos no se observa ninguna disminución sustancial de las tres eficiencias clave (coulómbica, tensión y energía). Esta prueba se realizó en ciclos de media hora.

En relación a la **metodología**:

La metodología propuesta ha sido desarrollada por Moore et Al. e inspirada en un procedimiento jerárquico por pasos ideado por Douglas. Douglas [14] propone una metodología de varios pasos que incluyen heurísticas para el diseño de un sistema químico. Este método se diseña de forma aditiva de manera que si se detecta la inviabilidad económica del sistema en uno de los pasos (los denominados niveles) el procedimiento se detiene y se llega a la conclusión de la inviabilidad. La misma filosofía se utiliza en el enfoque de Moore [42]. Los costes pueden clasificarse en tres áreas: [14]

- Costes proporcionales a la capacidad energética
- Costes proporcionales a la capacidad energética
- Costes que no varían con el tamaño (el sistema de control y el equilibrio de la planta).

El método propuesto por Moore [42] estudia seis niveles diferentes:

- Nivel 1. Información de entrada para el VRB
- Nivel 2. Análisis entrada-salida

- Nivel 3. Consideraciones sobre la capacidad de potencia
- Nivel 4. Consideraciones sobre la capacidad energética

Durante el procedimiento se anualizan los costes. A continuación, se presentan los resultados de acuerdo a los niveles estudiados:

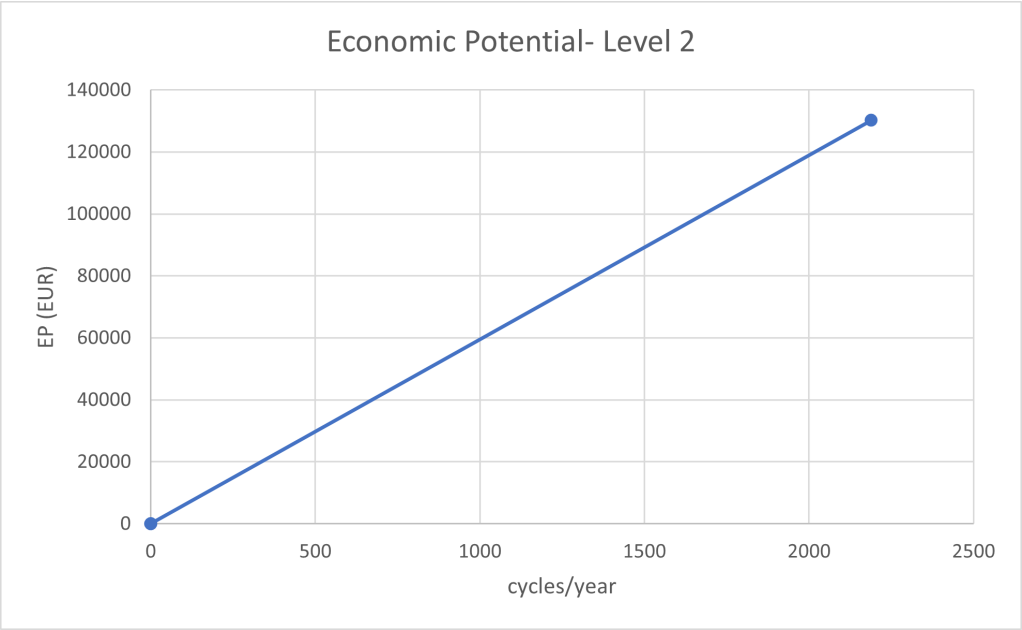

Figure 15 Potencial económico de Nivel 2.

Desafortunadamente, ya en el Nivel 3 este sistema deja de ser económicamente viable.

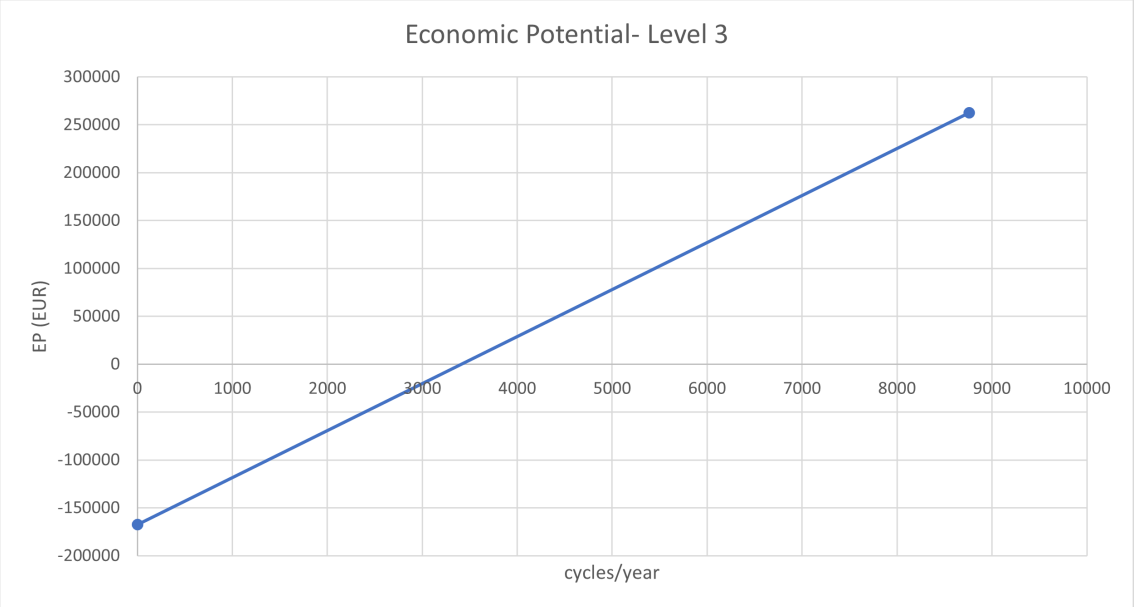

Figure 16 Potencial económico de nivel 3.

De ella se desprende que el punto en el que la batería se vuelve viable es a partir del ciclo número 3413.

No obstante, se calculan los costes del resto de equipamiento relacionado (Ánalisis de nivel 4) y se obtiene la siguiente distribución de costes, que se compara con otras distribuciones derivándose las siguientes conclusiones:

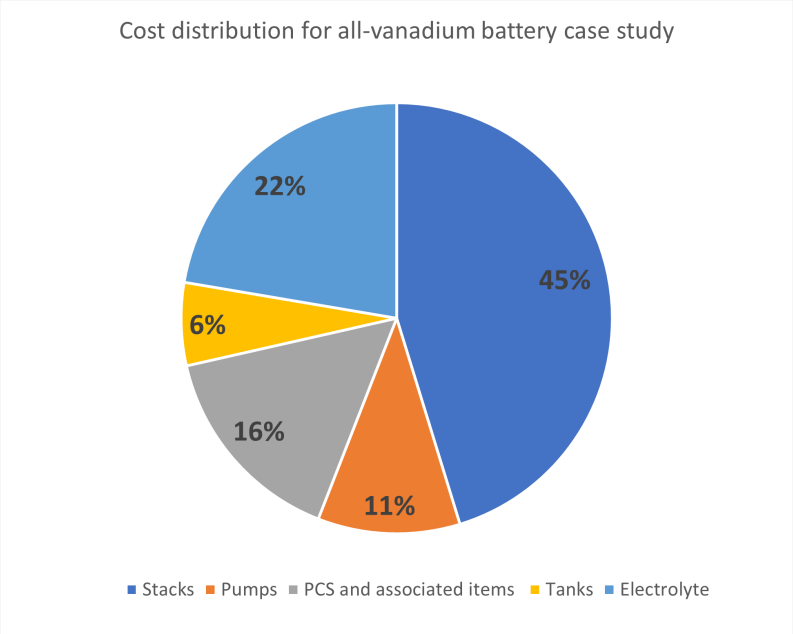

Figure 17 Distribución de costes para el caso de estudio.

Como se muestra a continuación, el coste distribuido del electrolito oscila entre el 8% para un cuarto de hora de duración de la batería y el 43% para cuatro horas de duración de la batería. En el estudio que se ha realizado, la bateríaes de 2 horas y el porcentaje de coste atribuido es del 22%, situándose dentro de este rango. Del mismo modo, el coste de los depósitos es en ambos análisis el coste porcentual más bajo de todo el sistema. Por tanto, se puede concluir que las pilas y el electrolito de la batería suponen la mayor parte del coste en ambos casos. El PCS, los depósitos y las bombas contribuyen al coste total, pero no suponen una gran cantidad de dinero en la inversión. El porcentaje atribuido al pentóxido de vanadio es proporcional a la duración de la batería. Además, también cabe señalar que la pila de celdas constituye en el análisis de Viswanathan [71] un porcentaje del 60% y el 73% se debe al separador en el sistema de baterías de 0,25 MWh. Del mismo modo, para el sistema de 4 MWh, el 38% del coste pertenece a la pila de celdas y el 71% a al separador. En el caso de estudio presentado a lo largo del análisis, las cifras siguen siendo similares, con un El 45% se atribuye a la pila de celdas y el 62,3% se debe al IEM. Estas conclusiones comparten descubrimientos sobre la distribución de costes de los componentes entre diferentes sistemas.

5. Conclusión

Este trabajo expone los problemas y retos que plantea el desarrollo y la investigación de las baterías de flujo redox. Esta tecnología pionera abre una vía para resolver problemas que requieren un sistema de baterías, como la nivelación de la carga o la estabilización de la frecuencia. Sobre todo, parece prometedora y necesaria dada la casi obligatoria entrada en el mercado de fuentes de energía renovables para contrarrestar los efectos de la quema de combustibles fósiles como fuente de energía (estos últimos son causa de contaminación y su uso incesante provoca efectos irreversibles en el cambio climático). Sin embargo, la continuidad del suministro nunca está garantizada utilizando recursos energéticos renovables. De este modo, las baterías proporcionan un medio de almacenar energía y emplearla cuando una fuente de energía renovable no la está produciendo (por ejemplo, por la noche en el caso de los paneles fotovoltaicos).

Como ya se ha comentado, existen muchos modelos de baterías que compiten con las baterías de flujo redox. En términos generales, estos tipos de baterías consisten en una tecnología más madura y tienen una mayor densidad energética, lo que las hace más deseables para una amplia gama de aplicaciones.

Se han realizado esfuerzos para mejorar el rendimiento de las baterías de flujo redox. La mayoría de las líneas de investigación interesantes se han dirigido a mejorar la eficiencia energética (tanto la eficiencia coulómbica como la eficiencia de voltaje), pero pocas líneas de investigación investigan la estabilidad de un sistema de baterías. Aunque la mejora de la eficiencia pueda parecer más atractiva desde el punto de vista de la investigación, este último punto es crucial para que los sistemas sean comercial e industrialmente viables. Sin embargo, se necesita un tiempo considerable para demostrar la estabilidad a largo plazo de un sistema.

La mayoría de las líneas de investigación se centran entonces en mejorar una de las partes cruciales que conforman una batería de flujo redox para demostrar una mayor eficiencia. Es el caso de los grupos funcionales que se añaden a los electrodos o la gran cantidad de tratamientos a los que se han sometido diversos tipos de membranas. Existen múltiples configuraciones y la mayoría de ellas son temas vivos de investigación. Sin embargo, las baterías de todo vanadio parecen ser la tecnología más comercializada, con la instalación de grandes sistemas industriales. Esto se debe a que no es posible la contaminación por mezcla cruzada, ya que ambos electrolitos contienen las mismas especies. Aún queda mucho por hacer para mejorar la densidad energética de estos sistemas, así como los costes asociados.

Para comprobar este último punto, se ha realizado un análisis de un sistema técnicamente viable y estable que ya se está instalando en Japón. Los resultados de este análisis demuestran que no

son económicamente viables. En países como Estados Unidos, existe una mayor diferencia entre el coste de la electricidad en horas punta y en horas valle (una es unas diez veces mayor que la otra, a diferencia de España, donde es sólo el doble). Por lo tanto, la instalación de un sistema de baterías de flujo redox en esta red puede suponer un resultado positivo para la viabilidad. Por otra parte, la distribución porcentual de los costes de capital muestra que la membrana y las soluciones electrolíticas son los elementos más caros de un sistema totalmente de vanadio. Definitivamente, el volumen del electrolito representa un porcentaje mayor o menor de los costes en función de la duración de la batería.